Reducing conflicting forces with co-adaptive haptic shared control using online time-varying operator identification

MSc Thesis

J.E. Vos

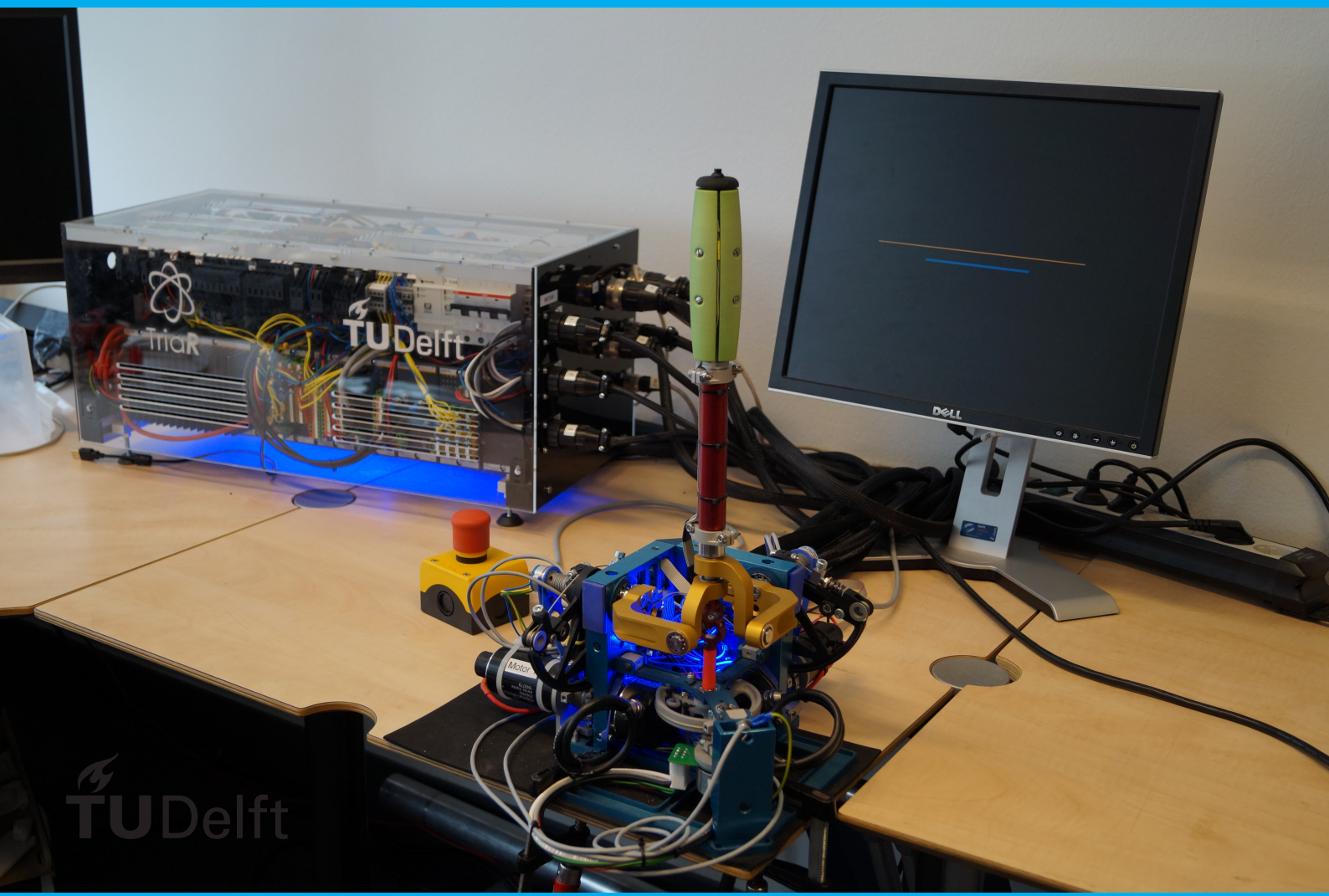

Reducing conflicting forces with co-adaptive haptic shared control using online time-varying operator identification

MSc Thesis

by

J.E. Vos

to obtain the degree of Master of Science
at the Delft University of Technology,
to be defended publicly on Thursday April 19, 2018 at 1:00 PM.

Student number:	4153138	
Project duration:	June 23, 2017 – April 19, 2018	
Thesis committee:	Prof. dr. ir. D.A. Abbink,	TU Delft, supervisor
	Dr. ir. D.M. Pool,	TU Delft
	Dr. ir. S.M. Petermeijer,	TU Delft

An electronic version of this thesis is available at `http://repository.tudelft.nl/`.

TU Delft

CONTENTS

List of Figures

List of Tables

Reducing conflicting forces with co-adaptive haptic shared control using online time-varying operator identification

J.E. Vos, BSc Dr. ir. D.M. Pool Dr. ir. S.M. Petermeijer Prof. dr. ir. D.A. Abbink

***Abstract*—Haptic shared control (HSC) is a method to combine the abilities of humans and machines, in which human and automation jointly exert forces on an input device. According to human-centered design, the underlying controller for HSC should closely resemble human behavior. This paper aims to continuously adapt HSC based on an online identified operator model. This approach is named co-adaptive HSC. Co-adaptive HSC is hypothesized to decrease conflicts when the human adjusts his control behavior to changing requirements of the task.**

In a compensatory tracking experiment with eleven participants, co-adaptive HSC is compared to time-invariant HSC. During the experiments, the participants control a time-varying controlled element, which changes from a single integrator to a double integrator and back unannounced. Time-invariant HSC was designed for controlling a single integrator, whereas co-adaptive HSC adapted to the human by continuously estimating the time-varying parameters of the operator using an Extended Kalman Filter (EKF). This online identified model of the operator was directly used in the shared controller, therefore, the co-adaptive HSC imitates human behavior.

A 36% decrease in conflict rate (the percentage of time in which the human force and the controller force have opposite directions) was found for co-adaptive HSC compared to time-invariant HSC when the controlled element was a double integrator. However, for some participants incorrect EKF-estimation of the neuromuscular damping resulted in undesired oscillations in control force during co-adaptive HSC. This indicates that the performance of co-adaptive HSC can be further improved.

Overall, this study proves that co-adaptive HSC is a promising method to reduce conflicts, and is able to adapt to operator behavior in unforeseen situations.

I. Introduction

To facilitate effective human-machine interaction, Billings introduced guidelines for human-centered automation, suggesting that automation should keep the human involved in the task [1]. Furthermore, both the human and automation should have knowledge of the other's intent and the automation should perform the task in a manner similar to the human. These guidelines have been used in shared control for various applications (i.e. adaptive cruise control design [2], collaborative sawing tasks [3], and point-to-point tasks [4]).

In the driving domain, haptic shared control (HSC) was developed in different groups as a way to combine the capabilities of humans and automation [5]–[8]. Both the human and the haptic shared controller exert torques on the steering wheel. This allows the human and the HSC to continuously interact and communicate through haptic feedback, while at the same time collaboratively controlling a vehicle.

HSC has shown to improve lane-keeping performance [6]–[10] and decrease control activity [6], [7], [10] compared to manual control. However, conflicting torques are also reported [6], [10], which can lead to annoyance, discomfort and dangerous situations [11]. Resolving such conflicts could lead to increased acceptance of shared control systems [12].

Adapting automation to individual operators potentially reduces conflicts. Automation can be individualized offline using manual control data [3], [12], [13]. However, behavioral adaptation is seen for human operators in various tasks [14], especially when HSC is implemented [15], [16]. This means an operator model identified offline will no longer accurately predict human behavior during shared control trials. As a result, conflicts will remain to exist, because discrepancies between the human strategy and the controller strategy are not permanently avoided.

A strategy to resolve conflicts even further would be to update HSC continuously based on an operator model identified online. When using this type of HSC, the human adapts its behavior to the HSC and the HSC, in turn, adapts its behavior to the human, see Figure 1. This process is called *co-adaptation*. If co-adaptation is successful, the human behavior and HSC behavior will be equal and no conflicts are present. This means that the human and the HSC will both contribute half of the required forces.

Trial-by-trial co-adaptation has been implemented for various applications (i.e. a free air tele-operation task [17], a collaborative point-to-point task [4], a human assisted robot standing up task [18], and collaborative table carrying task [19]). In these examples, convergence of human and automation behavior was seen. To the authors' knowledge, however, co-adaptation has always been applied incrementally between trials, not continuously (i.e. online) during the execution of a task.

The objective of this study is to develop continuous co-adaptive HSC in a tracking task setting. A compensatory tracking task is used to allow for established operator models [20], [21], and online time-varying parameter estimation [22], [23] to be used. In order to force time-varying operator behavior, the controlled element is made time-varying, changing from a single integrator to a double integrator and back during the task [21], [24]. A block scheme

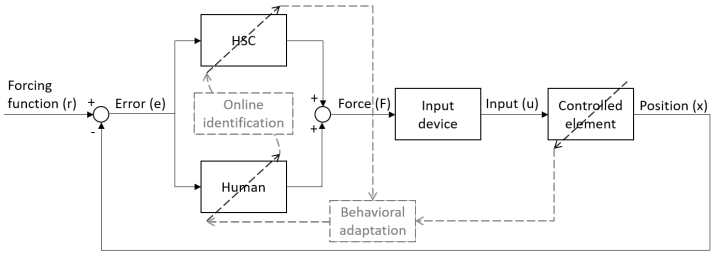

Fig. 1: A block scheme of the compensatory tracking task. The error (e), which is calculated from the forcing function (r) and the current position (x), is shown on the screen to the human and used as an input for the HSC. Both the human and the HSC exert forces (F) on a joystick (the input device). The joystick angle (u) is used as an input for the controlled element. The controlled element changes from a single integrator to a double integrator and back. The changes in controlled element dynamics and HSC behavior lead to adapted operator behavior. Online time-varying parameter estimation is used to model the operator and adapt the HSC. Co-adaptation is present as both the human and the HSC adapt to each other.

of this task is visualized in Figure 1. Co-adaptive HSC is compared to time-invariant HSC, designed for controlling a single integrator, and *a priori* optimized HSC, which is a best-case scenario using *a priori* knowledge of the changes in controlled element dynamics. A comparison will be made in terms of conflicts, task performance, control effort and control activity. In this paper, the definition of a *conflict* is that the human force and the HSC force have opposite directions.

The hypothesized changes in conflict rates (percentage of time a conflict is present) are the following. In unforeseen situations, both *a priori* optimized HSC and co-adaptive HSC lead to a reduced conflict rate compared to time-invariant control. In transient phases, *a priori* optimized HSC has the advantage of *a priori* knowledge and outperforms co-adaptive HSC. More formally stated:

Hyp1 When the controlled element is a double integrator, *a priori* optimized HSC results in lower conflict rates than time-invariant HSC.

Hyp2 In steady-state situations with a double integrator as the controlled element, co-adaptive HSC results in lower conflict rates than time-invariant HSC.

Hyp3 In transient phases, co-adaptive HSC results in higher conflict rates than *a priori* optimized HSC.

The remainder of this paper is structured as follows. The HSC design is discussed in Section II, followed by an explanation of the methodology in Section III. Section IV contains the results of the experiment, which are discussed in Section V. The paper ends with a conclusion in Section VI.

II. HSC DESIGN

In this paper, three types of HSC are compared. All HSC types attempt to reproduce human operator behavior using the same human operator model as a control law. However, the (time-varying) parameters of this model are different for every condition. The HSC is gradually switched on using a ramp function between 10 and 15 seconds for every HSC type. Time-invariant HSC is developed for controlling a single integrator, *a priori* optimized HSC is developed for the exact time-varying controlled element dynamics of this study and co-adaptive HSC adapts online to the current operator behavior. For the development of time-invariant HSC and *a priori* optimized HSC, a prestudy was conducted with four participants.

A. Human operator model

McRuer and Jex introduced a quasilinear human operator model [20], which was later extended with neuromuscular parameters [25]. To be able to capture human behavior during control of a single integrator as well as control of a double integrator, [21] used the transfer function shown in (1).

$$H_p(s,t) = \overbrace{(K_{dot}(t)s + K_e(t))}^{\text{Equalization}} \cdot \underbrace{e^{-s\tau(t)} \frac{\omega_{nms}(t)^2}{\omega_{nms}(t)^2 + 2\zeta_{nms}(t)\omega_{nms}(t)s + s^2}}_{\text{Limitations}} \quad (1)$$

where K_e is a gain on the error and K_{dot} is a gain on the derivative of the error. These parameters are referred to as equalization parameters. Time delay τ [s] and neuromuscular parameters ζ_{nms} [Ns/rad] and ω_{nms} [rad/s] introduce limitations for the operator behavior. This model predicts the joystick angle using the error as an input. However, implementation of HSC requires a model that predicts operator force. Therefore, in this study, the model is extended with a simple inverse joystick model. To prevent the total transfer function from becoming improper, the joystick is modeled using a spring and a damper (thus neglecting the mass). The fit of the joystick model in the frequency domain can be seen in Appendix G. The resulting pilot model is shown in (2).

$$H_p(s,t) = \overbrace{(K_{dot}(t)s + K_e(t))}^{\text{Equalization}} \cdot \underbrace{\frac{e^{-s\tau(t)}\omega_{nms}(t)^2}{\omega_{nms}(t)^2 + 2\zeta_{nms}(t)\omega_{nms}(t)s + s^2}}_{\text{Limitations}} \cdot \underbrace{\frac{Bs + K}{1}}_{\substack{\text{Inverse} \\ \text{joystick model}}} \quad (2)$$

where B [Ns/rad] is the joystick damping and K [N/rad] is the joystick stiffness.

B. HSC types

HSC_{TI} For time-invariant HSC, a parametric model is made for the mean frequency response during steady-state control of a single integrator. These parameters are used as HSC parameters.

HSC_{APO} For *a priori* optimized HSC, a parametric model is made for the mean frequency response of the behavior during steady-state control of a single integrator and during steady-state control of a double integrator. The parameters are varied using the scheduling function described in Section III-A2. The joystick parameters from time-invariant HSC are taken.

HSC_{CA} For co-adaptive HSC, the control law is continuously adapted to the operator behavior. For this type of HSC, the operator model parameters should be estimated online.

The parameters for time-invariant and *a priori* optimized HSC and their fits in the frequency domain are shown in Appendix G.

C. Online time-varying human operator identification

Identification in the frequency domain is impractical for online implementation because averaging cannot be used [23]. In the time domain, recursive methods are used to estimate operator model parameters. [24] used recursive least squares with an autoregressive exogeneous model (ARX) on manual control data. Extended Kalman Filters (EKF) have also been used [22], [23], [26]. In this study, an EKF will be used to identify the parameters of the operator model, as it is flexible with regard to the model structure [22], which is beneficial when extending this research to other applications.

The human operator model as described in (2) contains seven parameters. Three of those (τ, B, and K) are estimated offline using manual control data and assumed to be constant. The estimation procedure is explained in Appendix H.

An EKF is used to estimate the four remaining parameters online (K_{dot}, K_e, ω_{nms}, and ζ_{nms}). The settings of the EKF (P-matrix, Q-matrix, and R) were tuned based on prestudy data, with the objective of maximizing the variance accounted for (VAF). A detailed description of the EKF is presented in Appendix E and simulation results are shown in Appendix F.

Identified parameters are directly fed through to the control law. However, negative estimated parameters are changed into zero.

III. Methods

A. Experimental set-up

A one-dimensional compensatory tracking task was performed, based on the experiment described by [21]. A block scheme of the task is shown in Figure 1.

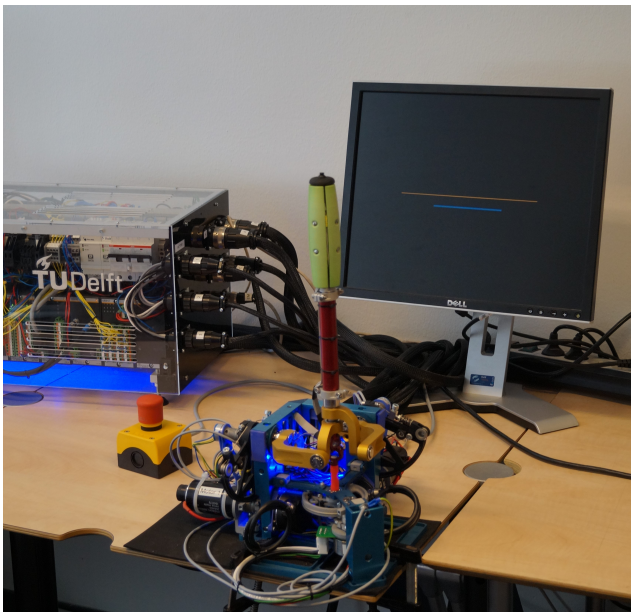

Fig. 2: Experimental set-up. The TriaR joystick is seen, with an emergency button and the Bachmann real-time computer in the background. On the screen, the orange line represents the reference and the blue line represents the current error.

1) Hardware: The joystick that was used for the experiment is the TriaR joystick with three degrees of freedom (DOF) [27]. A photo of the experimental set-up is shown in Figure 2. For this experiment, only the forward-backward DOF is used. Rotation around the z-axis was physically prevented. Rotation in the left-right direction was prevented by implementing a high passive stiffness (100 N/rad) combined with a passive damping (0.2 Ns/rad). The passive stiffness and damping in the relevant direction were 8 N/rad and 0.4 Ns/rad respectively. The joystick is controlled at a rate of 1 kHz by a dedicated Bachmann real-time computer. A desktop computer sampled the error at 30 Hz and displayed the error on a screen. Data was logged at the Bachmann computer with a sampling rate of 1 kHz, and downloaded to the desktop computer after every trial.

2) Controlled element dynamics: In the original experiments of McRuer and Jex, a gain, a single integrator, and a double integrator were considered as the controlled element [20]. In this study, the controlled element dynamics are time-varying, thereby forcing the operator to adapt his behavior. To implement controlled element dynamics that change from a single integrator to a double integrator and back, an approximation was proposed in [21]. The transfer function belonging to this approximation is shown in (3). By increasing or decreasing ω_b, this transfer function approaches a single integrator or a double integrator, respectively.

$$H_{CE}(s,t) = \frac{K_c(t)}{s^2 + \omega_b(t)s} \tag{3}$$

The gain K_c and break frequency ω_b are time-varying parameters. For an approximation of a single integrator, K_c is equal to 90 and ω_b is equal to 6 rad/s. For

TABLE I: Experimental design: order of the trials

	Conditions			
Training 1	40-second manual control trials with a single integrator*			
Training 2	40-second manual control trials with a double integrator*			
Training 3	manual control for offline identification		manual control for validation	
Block 1	time-invariant HSC	co-adaptive HSC	*a priori* optimized HSC	manual control
Block 2	*a priori* optimized HSC	manual control	co-adaptive HSC	time-invariant HSC
Break	fifteen minutes			
Block 3	manual control	*a priori* optimized HSC	time-invariant HSC	co-adaptive HSC
Block 4	co-adaptive HSC	time-invariant HSC	manual control	*a priori* optimized HSC

* until the increase in performance is less than 5% compared to the previous trial

approximating a double integrator, K_c is equal to 30 and ω_b is equal to 0.2 rad/s [21]. During the experiment, the controlled element changes from a single integrator to a double integrator and back. The first transition is defined by a sigmoid function, see (4). The transition back to a single integrator is modeled as a step change.

$$P(t) = P_1 + \frac{P_2 - P_1}{1 + e^{-G(t-M)}} \tag{4}$$

where $P(t)$ is a time-varying parameter function, changing from an initial value P_1 to a final value P_2. The maximum rate of change G is equal to 0.5 s^{-1}, the moment in time where the maximum rate of change occurs (M) is equal to $t = 70$ s. This results in a smooth sigmoid-shaped transition that occurs between 60 and 80 seconds. The controlled element parameters used during the experiment are shown in Figure 3.

3) Forcing function: A multisine is used as the forcing function. The design of the multisine in inspired by the procedure explained in [21], [28]. The multisine is a sum of ten individual sines, as shown in (5).

$$f(t) = \sum_{k=1}^{10} A(k) \sin\left(\omega(k)t + \phi(k)\right) \tag{5}$$

where $A(k)$ is the amplitude, $\omega(k)$ is the frequency in rad/s and $\phi(k)$ is the phase shift in rad. In order to be able to use frequency domain analysis methods for the steady-state segments (1, 3, and 5 in Figure 3), the period of the multisine (T_m) is 40 seconds. The frequencies $\omega(k)$ are all integer multiples (n) of the base frequency $\omega_{\text{base}} = 2\pi/T_m = 0.1571$ rad/s. The frequencies cover the range relevant to human control behavior (0.1-18 rad/s) [21]. The frequencies are approximately logarithmically spaced between ω_{base} and 18 rad/s. The amplitude of the individual sinusoids is calculated using (6). This results in a bandwidth of approximately 0.81 rad/s. The final multisine is scaled in order to ensure the amplitude is equal to a quarter of the screen height.

$$A(k) = \left| \frac{\left(1 + 0.1j\omega(k)\right)^2}{\left(1 + 0.8j\omega(k)\right)^2} \right| \tag{6}$$

To determine the phase shifts in (5), 2000 random combinations of phase shifts are generated. Using those phase shifts, 2000 multisines are computed and the multisine with a probability distribution closest to a normal distribution was chosen. Normality was assessed using a χ^2-test [28]. The properties of the resulting multisine forcing function are listed in Table II.

For each trial, the starting point of the forcing function is randomly shifted within a five-second window, to make the changes in controlled element dynamics unpredictable.

TABLE II: Properties of the forcing function

k	n	$\omega(k)$ [rad/s]	$A(k)$	$\phi(k)$ [rad]
1	1	0.1571	0.9847	3.2020
2	2	0.3142	0.9415	0.0461
3	3	0.4712	0.8775	2.7465
4	4	0.6283	0.8015	2.2040
5	6	0.9425	0.6432	1.1241
6	11	1.7279	0.3538	3.6919
7	20	3.1416	0.1502	4.8932
8	36	5.6549	0.0615	2.2005
9	64	10.0531	0.0306	6.1250
10	114	17.9071	0.0204	3.9537

B. Experimental protocol

This study was approved by the Human Research Ethics Committee of the Delft University of Technology (see Appendix D).

The experiment was conducted based on a within-subjects, repeated-measures design. The participants performed four repetitions of four conditions: manual control, time-invariant HSC, *a priori* optimized HSC and co-adaptive HSC. The conditions were counterbalanced across repetitions using a Latin square to reduce the influence of learning effects [29]. The order of the conditions is shown in Table I and was the same for each participant. Before the actual experiment, a training phase was completed to reduce the learning effects during the experiment. In the last training block, B, K, and τ were estimated offline. Another trial was performed to validate that the EKF was able to replicate human behavior. If the variance accounted for, see (7), between human force and EKF-expected force was higher than 50%, the actual experiment was started. This requirement was met by all subjects.

After every experimental trial, the participants rated the usefulness and satisfaction of the condition using the Vanderlaan questionnaire [30]. During both the training phase and the actual experiment, participants were notified of their performance (in term of the root mean square error) after every trial.

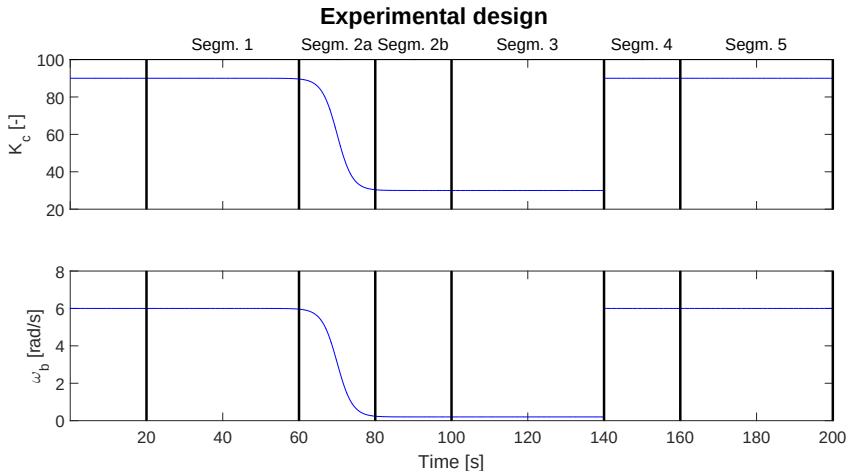

Fig. 3: Controlled element parameters K_c and ω_b over time. The experimental data will be analyzed in six segments. Segments 1, 3, and 5 represent steady-state behavior, segments 2a, 2b, and 4 represent transient behavior of the human operator.

C. Task instruction

The goal of the task is to minimize the error between the position (x) and the forcing function (r), see Figure 1. The blue horizontal line on the screen shows the current error, see Figure 2. Rotation of the joystick in the forward-backward direction corresponded to a movement of the blue line in an upward-downward direction, respectively.

The participants read an experimental briefing explaining the experiment. In this briefing, the participants were asked to perform the tracking task to the best of their abilities. The briefing also stated that the haptic shared control "may or may not be correct and useful", and that it is the "objective [...] to minimize the error shown on the screen, regardless of the guidance". After reading the briefing, the participants signed an informed consent form. Next, the participants filled out a general questionnaire including questions about age, gender, and previous experience in tracking tasks. The experimental briefing, informed consent form, and general questionnaire are attached as Appendices A, B, and C, respectively.

D. Dependent variables

Before analysis, the data was down-sampled to 100 Hz. The data was analyzed separately for the six trial segments, see Figure 3. The following metrics were calculated for each participant and each condition. An average value was determined using the four repetitions.

- **RMSE** The root mean square error [-] between the position and the forcing function was calculated as a measure of task performance.
- **RMSU** The root mean square joystick angle [radians] was used as a measure of the control activity.
- **Mean‖F‖** The mean absolute control force [Newton] was used as a measure of the control effort.
- **Conflict rate** The percentage of time during which the human force and the controller force have an opposite direction was used as a measure of conflicts.
- **VAF** The variance accounted for [%] was used as a measure of the quality of the identified operator model. The VAF between the human force and the expected force was used to assess the identification quality. VAF can be calculated using Equation 7.
- **Usefulness** The usefulness was calculated from the results of the Vanderlaan questionnaire.
- **Satisfaction** The satisfaction was calculated from the results of the Vanderlaan questionnaire.

$$\text{VAF} = \left(1 - \frac{\text{Var}(F_{\text{human}} - F_{\text{expected}})}{\text{Var}(F_{\text{human}})}\right) \cdot 100\% \quad (7)$$

E. Statistical analysis

The first step in the statistical analysis is to analyze the normality of the data using the Shapiro-Wilk test [31]. In case the data was normally distributed, it was submitted to analysis of variance (ANOVA) [32] with the four conditions as the within-subjects factor. Mauchly's sphericity test was used to assess the sphericity [33], if the sphericity criterion was not met, a Greenhouse-Geisser correction was performed [34]. Bonferroni corrected post-hoc t-tests were used to evaluate differences between conditions [35]. If the normality assumption was not justified, a Friedman test was used [36], followed by Bonferroni corrected Wilcoxon post-hoc tests [37]. For all statistical analyses, a significance level of α = 0.05 was used.

F. Subjects

Eleven male students of Delft University of Technology were recruited to participate in the experiment. Ten out of eleven participants were right-handed, all participants had normal or corrected-to-normal vision. The average age was 24.6 years, with a standard deviation of 1.3 years. The subjects did not receive any financial compensation for their participation.

TABLE III: Joystick parameters (B and K) and operator time delay (τ) estimated offline

	Mean	Standard deviation
B [Ns/rad]	0.879	0.186
K [N/rad]	7.464	0.198
τ [s]	0.347	0.086

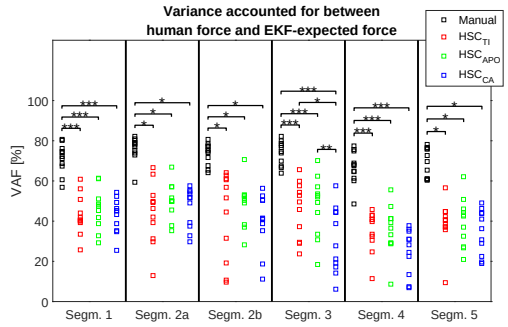

Fig. 4: Variance accounted for between human force and expected force based on the EKF identification during all trials. The stars represent significance, one star means $p \leq 0.05$, two stars mean $p \leq 0.01$, and three stars mean $p \leq 0.001$.

IV. Results

A. Parameter estimation

The average offline identification results of the joystick parameters (B and K) and human time delay (τ) are listed in Table III. The average online identification results for K_{dot}, K_e, ω_{nms}, and ζ_{nms} for all conditions are shown in Appendix I. The VAFs for all conditions are shown in Figure 4. VAFs for manual control trials are significantly higher than VAFs for shared control trials in all segments. Co-adaptive HSC results in the lowest VAFs. When averaged over participants and segments, the mean VAFs for manual control and co-adaptive HSC are 71.6% and 43.4%, respectively.

In Figure 5, the average identified parameters are shown after the initial transient of 20 seconds. The shaded area represents the standard deviation over participants. Both human gains (K_{dot} and K_e) are approximately a factor two lower for co-adaptive HSC compared to manual control. For the neuromuscular damping, the average identification results are approximately equal, while the standard deviation over participants is higher for co-adaptive HSC. The neuromuscular frequency is estimated to be 12% lower for co-adaptive HSC compared to manual control. Adaptation of the identified parameters mostly occurs within the predefined transient segments 2a, 2b and 4. The identified operator parameters (averaged over participants) are approximately constant within segments 1, 3 and 5.

B. Conflicts, task performance, and control inputs

The performance of the haptic shared controllers is evaluated based on task performance, control effort, control activity, and conflicts. Task performance is not influenced by HSC conditions, see Figure 6(a). Control effort, however, is significantly reduced in all HSC conditions, see

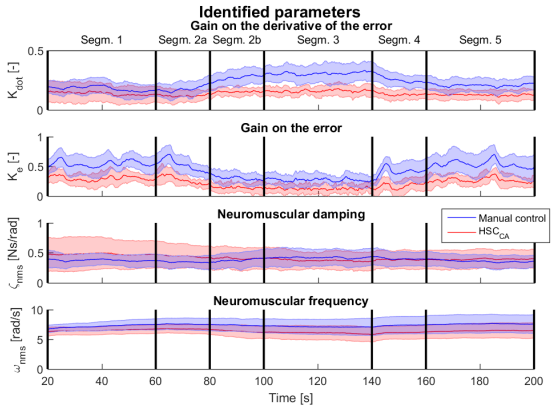

Fig. 5: Mean estimated parameters after an initial transient of 20 seconds for manual control trials and co-adaptive HSC trials. The solid lines represent the mean estimated parameters at every point in time, shaded areas represent the standard deviation over participant's means.

Figure 6(b). In segment 3, control activity for co-adaptive HSC is significantly higher than during manual control and *a priori* optimized HSC, see Figure 6(c). This is caused by two high values, for participant 11 and participant 2. Those participants will be studied in more detail in the Section IV-D. Significant differences exist for the conflict rate when the controlled element is a double integrator (segments 2b and 3), $F(1.30, 12.98) = 17.37$, $p \leq 0.001$ and F(1.21, 12.08) = 28.28, $p \leq 0.001$ respectively, see Figure 6(d). More specifically, in segments 2b and 3, co-adaptive HSC (blue) realized a 39% ($p \leq 0.05$) and 36% ($p \leq 0.01$) reduction in conflict rate, respectively, compared to time-invariant HSC (red). Over the course of the entire trial, co-adaptive HSC resulted in a 19% lower conflict rate compared to time-invariant HSC, whereas *a priori* optimized HSC resulted in a 20% reduction. No difference in conflict rate was found between co-adaptive HSC and *a priori* optimized HSC.

C. Subjective task evaluation

The conditions were also evaluated subjectively using the Vanderlaan questionnaire [30]. This questionnaire rates the usefulness and satisfaction of the different conditions. These results are presented in Figure 7. Overall, significant differences exist between all conditions for both satisfaction and usefulness ($F(3, 30) = 7.85$, $p \leq 0.001$ and F(1.27, 12.70) $= 6.59$, $p \leq 0.05$ respectively). However, Bonferroni corrected post-hoc tests revealed only a significant increase in satisfaction for *a priori* optimized HSC (green) compared to manual control (black) and time-invariant HSC (red), $p \leq 0.01$ and $p \leq 0.05$ respectively. Participants 2 and 11, who showed a high control activity in segment 3 for co-adaptive HSC, also gave a low rating for this condition on both satisfaction and usefulness. These participants will be studied in more detail in Section IV-D. Except for those scores, subjective data for co-adaptive HSC is not significantly worse than for *a priori* optimized HSC.

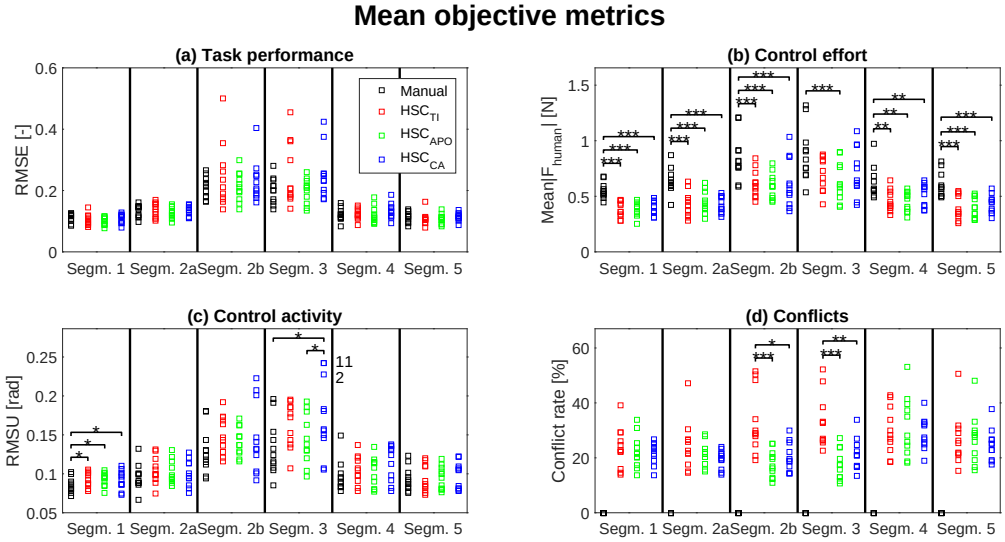

Fig. 6: Objective metrics for the four conditions, data points represent participant's means. The stars represent significance, one star means $p \leq 0.05$, two stars mean $p \leq 0.01$, and three stars mean $p \leq 0.001$.

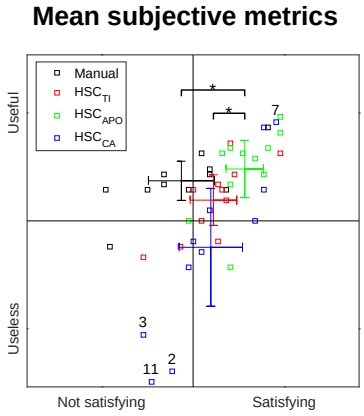

Fig. 7: Subjective metrics for the four conditions, data points represent participants' mean ratings. Error bars represent confidence intervals. For some data points for co-adaptive HSC, participant numbers are shown. The stars represent significance, one star means $p \leq 0.05$.

D. Exploratory analysis: co-adaptation

To study co-adaptation, exerted forces and estimated parameters are compared for two participants during and after the transition to a double integrator (segments 2a and 2b). Because large individual differences exist in both objective and subjective evaluation, no averages are used in this exploratory section. Results for participant 6, run 4 and participant 11, run 2 are shown in Figure 8 as representative examples.

During the first 20 seconds, the controlled element gradually changes from a single to a double integrator (segment 2a). In the last 20 seconds, the controlled element is a double integrator (segment 2b). For participant 6, the HSC force approximately follows the human force, although human behavior adapts during this time window. The co-adaptive HSC is able to adapt to the new behavior. In terms of identified parameters, it can be seen that K_{dot} increases slightly and K_e decreases during the transition, as expected [21]. A slight decrease in ω_{nms} is seen, while ζ_{nms} does not change substantially. All in all, the identified parameters have converged to the new operator behavior.

For participant 11, run 2, from 80 seconds onward, the HSC force shows an oscillation at a frequency of 1.15 Hz. Around 90 seconds, oscillations are observed where human force and HSC force are out-of-phase. In this case, the HSC is unable to reproduce the human behavior. The resulting HSC force does not match human intentions and consequently, the human starts counteracting the HSC force. In the parameters, the most obvious difference with participant 6 is the lower neuromuscular damping. The estimated damping is even negative for some amount of time. This results in a high gain for some frequencies.

The out-of-phase force oscillations can be identified using sliding window cross-correlation between human force and HSC force. If the sliding window cross-correlation is negative for lag $t = 0$, an out-of-phase oscillation is present [38]. 10 out of 44 co-adaptive HSC trials show those oscillations. Figure 9 shows the frequency response functions based on EKF identification results for those 10 trials, in the middle of the 10-second window with the lowest cross-correlation of the trial. The blue lines represent the frequency response function (FRF) of *a priori* optimized HSC. It can be clearly seen that oscillatory peaks are present between 1 and 1.5 Hz. Those peaks are caused by incorrectly estimating a low or negative estimated damping. The peaks can explain oscillations of the force because the controller will show a strong response at those frequencies.

The out-of-phase force oscillations only occurred for co-adaptive HSC, namely for participants 1 (1 run), 2 (3

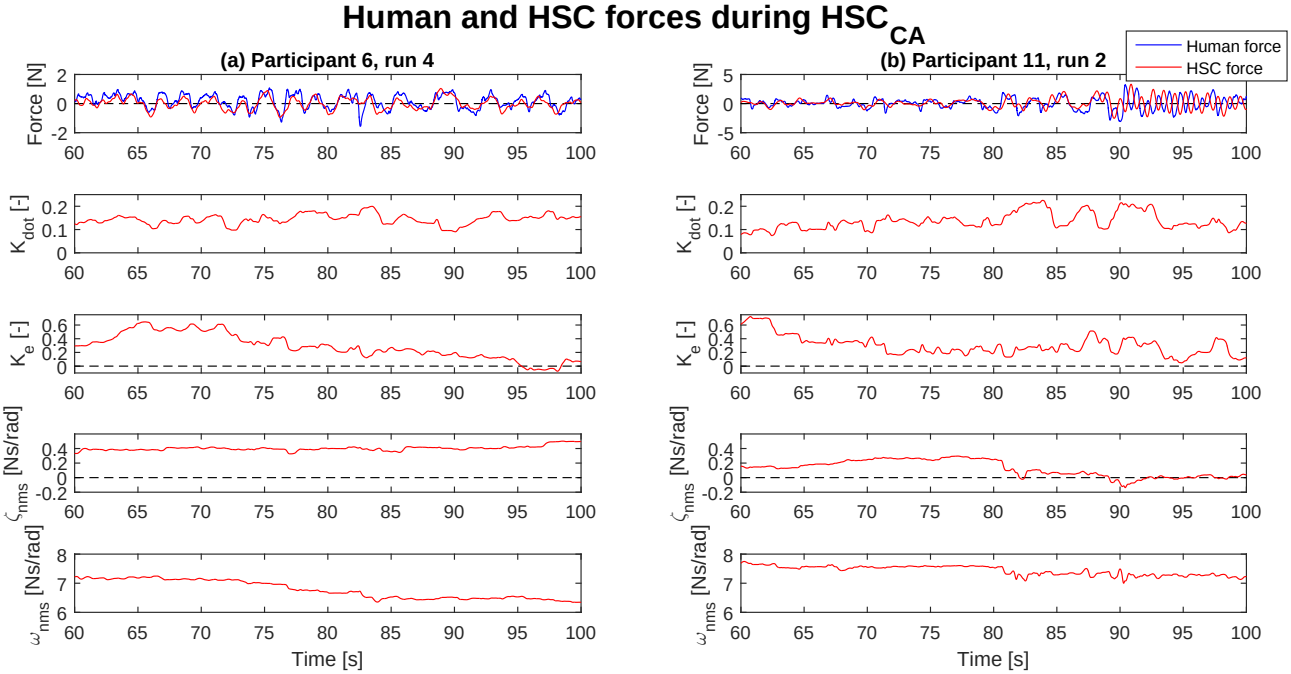

Fig. 8: Human and HSC force, and all estimated parameters for co-adaptive HSC for participant 6, run 4 and participant 11, run 2. The results are shown for segments 2a and 2b. For participant 6, the HSC adapts to the adapting human behavior. For participant 11, however, the HSC was unable to imitate human behavior and from 90 seconds onward, the human counteracts HSC force.

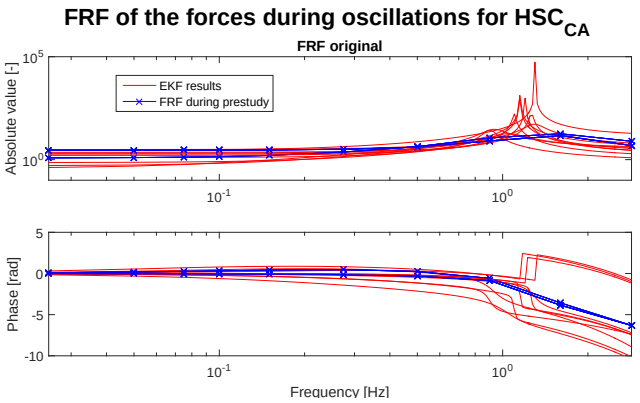

Fig. 9: Identified frequency response function (FRF) during the peak of out-of-phase oscillations. For all trials where out-of-phase force oscillations are seen, the FRF in the middle of the 10-second window with the lowest cross-correlation is plotted in red. The blue lines represent the FRF of *a priori* optimized HSC, where crosses mark the frequencies that are excited in the forcing function. Two blue lines are shown, representing *a priori* optimized HSC both when controlling a single integrator and when controlling a double integrator.

runs), 4 (1 run), 7 (2 runs), and 11 (3 runs). For participants 2 and 11, a low subjective rating and increased control activity were also seen. However, participant 7 still rates co-adaptive HSC as satisfying and useful.

V. Discussion

The objective of this study was to develop co-adaptive HSC in order to reduce conflicting forces. The conflict rate during the entire experiment was reduced by 19% compared to time-invariant HSC, indicating that this goal has been reached. However, this study also revealed that problems can arise when applying co-adaptive HSC in practice.

A. Performance

1) Conflicts, task performance, and control inputs: The primary aim of co-adaptive HSC was to reduce conflicts. In segments 2b and 3, the controlled element is a double integrator. Time-invariant HSC displays behavior that is meant for controlling a single integrator. This leads to increased conflict rates. A significant reduction in conflict rates is seen for *a priori* optimized HSC and co-adaptive HSC. Therefore, hypotheses 1 and 2 are confirmed. No significant difference between co-adaptive HSC and *a priori* optimized HSC in terms of conflicts rate is seen in any segment. Therefore, hypothesis 3 is rejected. Overall, this shows that co-adaptive HSC is able to converge to the desired behavior in various situations, without the need of *a priori* knowledge. In this study, the conditions were only balanced across repetitions, not balanced across participants. However, a post-hoc analysis revealed that learning effects did not have an effect on the conflict rate (see Appendix K for a detailed analysis).

No significant differences in task performance were found. This is probably caused by the fact that the controller has exactly the same strategy as a human operator. In HSC applications for lane-keeping tasks, an increase in performance is often reported [6]–[10]. However, in lane-keeping, humans show satisficing behavior [39]. This means that the human does not necessarily aim to keep

the center of the lane, while the controller does have this objective. As a result, HSC can improve lane keeping. In the task that is described in this study, the human shows less satisficing behavior, therefore, HSC does not significantly improve task performance.

However, HSC does significantly reduce the control effort in nearly all segments. Part of the force is delivered by the HSC, therefore, the human generally exerts less force on the joystick. This can directly be related to the reduction in both gains (K_{dot} and K_e). This means that a similar task performance is obtained for a lower control effort, showing the effectiveness of HSC. No significant differences in control effort were seen between HSC conditions.

Significant differences in control activity exist for some segments. However, in general, control activity is similar for all conditions. The differences in segment 1 are significant but very small. For segment 3, a significant increase in control activity is seen for co-adaptive HSC, which is caused by high control activity for participants 2 and 11. This is an indication that problems exist with co-adaptive HSC for those participants. Participants 2 and 11 also show out-of-phase force oscillations, see Appendix L.

2) Subjective metrics: For the subjective evaluation, the usefulness and satisfaction were assessed, see Figure 7. A large spread is seen, especially for co-adaptive HSC. This reflects the fact that large individual differences are present for co-adaptive HSC. *A priori* optimized HSC is rated more satisfying compared to time-invariant HSC and manual control. No significant differences exist between co-adaptive HSC and *a priori* optimized control. This means that, even though undesirable force oscillations were present for some participants, co-adaptive HSC is not rated significantly worse compared to the best case scenario.

B. Estimation results

1) Offline identified parameters: The average estimated value of τ is 0.347 seconds, which is higher than the values found in [21], which were around 0.25 seconds. If the time delay is estimated too high, the phase of the estimated model is too low at high frequencies. This can be partially corrected by estimating the neuromuscular damping too high. In its turn, this leads to a magnitude that is too low at high frequencies, which can be partially corrected by estimating the neuromuscular frequency too high. Therefore, inaccurate estimation of the time delay does not necessarily lead to low VAFs. Apparently, this is the case in this experiment, where the average VAF is 71.6% for manual control trials. The fact that the incorrect estimation of some parameters can be compensated for by the estimation of other parameters was also found in [23]. In future studies, however, more accurate offline estimation of the time delay would be beneficial. The most promising method to do this is to use more data for offline estimation.

The average estimated values for the joystick damping and stiffness (0.879 Ns/rad and 7.464 N/rad, respectively) are different from the impedance parameters (0.4 Ns/rad and 8 N/rad). Part of the increased damping is caused by friction in the joystick itself. The remainder of the differences is caused by the fact that there is a feedback loop from the joystick angle to the force containing grip dynamics, which is neglected in the model [14], [40]. The effect of this feedback loop can apparently be modeled as an increased damping and slightly decreased stiffness. The joystick model also holds during co-adaptive HSC, proving that B and K can indeed be estimated offline (see Appendix J for the frequency response function of the joystick during manual control and during co-adaptive HSC).

2) Online identified parameters: The duration of the transient of the identified parameters after a step change in the controlled element dynamics is roughly 15 seconds in the experiment, see Figure 5. The same is observed in simulation, where human adaptation is modeled as a step change, see Appendix F. This indicates that the human adaptation occurs quickly compared to the EKF dynamics. This might be the reason why convergence of the parameters was seen. If the controller would have adapted quicker, it would also be more sensitive and prone to oscillatory parameters. The effect of adaptation speed is subject to future work.

In simulation, estimating neuromuscular parameters is less reliable than estimating the gains, see Appendix F. An estimation bias for the neuromuscular frequency is found, which agrees with recent literature [23]. The difficulties in estimating neuromuscular parameters are probably caused by the interdependency between the artificial states of the system and those parameters. The negative estimated damping that leads to out-of-phase force oscillations is a result of the fact that estimating neuromuscular parameters is less reliable, proving it is important to improve the reliability of the estimation scheme.

The identified parameters during manual control and co-adaptive HSC show a similar trend, see Figure 5. Both estimated human gains (K_{dot} and K_e) are a factor two lower for co-adaptive HSC. Neuromuscular damping and frequency, however, are similar. During co-adaptive HSC, the operator model is directly used as a shared controller. This effectively doubles the gains, meaning that the combined gain for the human and the controller during co-adaptive HSC is similar to the gain for the human during manual control. This shows that the human and the HSC co-adaptively converge to human-preferred behavior.

3) Quality of fit: In manual control trials, the implemented EKF leads to an average VAF of 71.6%, with 83.3% of the VAFs between 60% and 80%. This closely corresponds with findings in [41], where it was found that the majority VAFs for offline identification of individual trials were between 60% and 80%. This indicates that the parameter estimation scheme is able to model time-varying human behavior for manual control trials. However, during shared control trials, the VAFs are substantially lower. During co-adaptive HSC, the average VAF is 43.4%. Apparently, modeling human behavior during HSC trials is

more difficult than it is during manual control trials. Low VAFs also indicate conflicts during co-adaptive HSC, as both metrics describe the similarity of human force and HSC force.

Although the VAF for co-adaptive HSC is lower than for manual control, the identified parameters are reasonable, see previous section. A possible explanation could be that human force during HSC trials is not only a reaction to the error shown on the screen, but also to the applied HSC force [14]. This dependency is not accounted for in the model. The fact that the model structure is incomplete for HSC trials, leads to more difficult estimation and lower VAFs. An effect of incorrect estimation during co-adaptive HSC trials is discussed in the next section.

4) Out-of-phase force oscillations: In 10 out of 44 co-adaptive HSC trials, incorrect estimation of neuromuscular damping leads to out-of-phase force oscillations. A low or negative estimated damping leads to an oscillatory peak in the FRF between 1 and 1.5 Hz (see Figure 9). Outside of this frequency range, the influence of neuromuscular damping is not seen. This also explains why estimating the neuromuscular damping was difficult; the forcing function did not contain power within this frequency range, therefore, the signal-to-noise ratio was low. This peak leads to an aggressive oscillatory response, which does not match human intentions. Therefore, the human starts to counteract this oscillation, which can be seen in Figure 8. From $t = 81$ s onward, the estimated damping is low or negative. This results in a force oscillation at approximately 1.15 Hz. Around $t = 90$ s, the human starts to counteract the force, resulting in an out-of-phase oscillation of the human and HSC force. Counteracting the force is probably done by the participants by using co-contraction. This way, a HSC force that does not correspond with human intentions directly results in a human exerted force in the opposite direction.

The out-of-phase force oscillation occurred most often for participants 2 and 11. Those participants also showed increased control activity and gave low subjective ratings. It is clear that those oscillations need to be prevented before co-adaptive HSC can be used.

5) Recommendations: Before co-adaptive HSC can be used in real-world applications, the robustness of the parameter estimation must be improved over what the currently implemented EKF provides. Apparently, parameter estimation that results in high VAFs for manual control trials is not sufficient. Multiple solutions are stated here, the effectiveness of which is subject to future work.

- A different parameter estimation scheme can be used. For example, a Double EKF can be used, where estimation of the states and the parameters are separated in order to improve the estimation [23].
- The signal-to-noise ratio can be improved in frequency ranges that are important for the estimation. In this experiment, the forcing function did not contain any power at the frequencies where neuromuscular damping is dominant. Including power at 1.2 Hz could possibly lead to improved robustness. This poses a problem for real-world applications, where the forcing function cannot be changed.
- Implementing upper and lower bounds for all parameters can reduce the risk of unsuccessful co-adaptation. However, this also requires some *a priori* knowledge.
- A model can be identified from the error on the screen to the joystick angle (similar to the original model [20]). Subsequently, the estimated model can be multiplied with the inverse joystick model to be able to compute HSC forces. Estimation results will now be less affected by the out-of-phase force oscillations, because the HSC force is canceled out by the human in those situations in order to let the joystick follow a human-preferred trajectory.
- It is beneficial to study which parameters are truly time-varying [14]. In this study, the neuromuscular parameters were found to be approximately constant. Estimating the neuromuscular parameters offline in the same way as time delay was estimated makes the online identification inherently more robust.

To estimate the parameters more accurately afterwards a Rauch-Tung-Striebel smoother could have been used [22], [42], combining both a forward and a backward recursive estimation. Using this method, the dynamics of the estimator can be partially counteracted. This method is advised for future research, because it makes it possible to study co-adaptation even more explicitly. However, this is not possible to implement in an online fashion.

VI. Conclusion

The aim of this study was to develop co-adaptive HSC and compare it to time-invariant HSC and *a priori* optimized HSC in a human-in-the-loop experiment. From the experiment, the following conclusions can be drawn:

- Accurate online time-varying parameter estimation during manual control trials does not guarantee robust co-adaptive HSC.
- Both co-adaptive HSC and *a priori* optimized HSC reduce the conflict rate compared to time-invariant HSC in time-varying situations.
- Co-adaptive HSC, not requiring *a priori* knowledge, performs equally good as *a priori* optimized HSC in terms of conflict rate.

This study proved that co-adaptive HSC can be used to substantially reduce conflicting forces in HSC without the need of *a priori* knowledge. Co-adaptive HSC performs equally good as the best case scenario with perfect knowledge.

References

[1] C. E. Billings, "Human-centered aircraft automation: A concept and guidelines," *Nasa Technical Memorandum*, no. February, 1991.

[2] M. A. Goodrich and E. R. Boer, "Model-Based Human-Centered Task Automation: A Case Study in ACC System Design," *IEEE Transactions on Systems, Man, and Cybernetics Part A:Systems and Humans.*, vol. 33, no. 3, pp. 325–336, 2003.

[3] L. Peternel, N. Tsagarakis, D. Caldwell, and A. Ajoudani, "Adaptation of robot physical behaviour to human fatigue in human-robot co-manipulation," *IEEE-RAS International Conference on Humanoid Robots*, pp. 489–494, 2016.

[4] T. Petrič, R. Goljat, and J. Babič, "Cooperative human-robot control based on Fitts' law," *IEEE-RAS International Conference on Humanoid Robots*, pp. 345–350, 2016.

[5] F. O. Flemisch, C. A. Adams, S. R. Conway, K. H. Goodrich, M. T. Palmer, and P. C. Schutte, "The H-Metaphor as a Guideline for Vehicle Automation and Interaction," *Control*, no. December, pp. 1 – 30, 2003.

[6] M. Mulder, D. A. Abbink, and E. R. Boer, "The effect of haptic guidance on curve negotiation behavior of young, experienced drivers," *Conference Proceedings - IEEE International Conference on Systems, Man and Cybernetics*, pp. 804–809, 2008.

[7] P. G. Griffiths and B. Gillespie, "Sharing control between humans and automation using haptic interface: primary and secondary task performance benefits." *Human factors*, vol. 47, no. 3, pp. 574–90, 2005.

[8] T. Brandt, T. Sattel, and M. Bohm, "Combining haptic human-machine interaction with predictive path planning for lane-keeping and collision avoidance systems," *2007 IEEE Intelligent Vehicles Symposium*, pp. 582–587, 2007.

[9] C. Blaschke, F. Breyer, B. Färber, J. Freyer, and R. Limbacher, "Driver distraction based lane-keeping assistance," *Transportation Research Part F: Traffic Psychology and Behaviour*, vol. 12, no. 4, pp. 288–299, 2009.

[10] M. Mulder, D. A. Abbink, and E. R. Boer, "Sharing Control With Haptics Seamless Driver Support From Manual to Automatic Control," *Human Factors: The Journal of the Human Factors and Ergonomics Society*, vol. 54, no. 5, pp. 786–798, 2012.

[11] M. Itoh, F. Flemisch, and D. Abbink, "A hierarchical framework to analyze shared control conflicts between human and machine," *IFAC-PapersOnLine*, vol. 49, no. 19, pp. 96–101, 2016.

[12] R. Boink, M. M. Van Paassen, M. Mulder, and D. A. Abbink, "Understanding and reducing conflicts between driver and haptic shared control," *Conference Proceedings - IEEE International Conference on Systems, Man and Cybernetics*, pp. 1510–1515, 2014.

[13] J. Wang, L. Zhang, D. Zhang, and K. Li, "An adaptive longitudinal driving assistance system based on driver characteristics," *IEEE Transactions on Intelligent Transportation Systems*, vol. 14, no. 1, pp. 1–12, 2013.

[14] M. Mulder, D. M. Pool, D. A. Abbink, E. R. Boer, P. M. Zaal, F. M. Drop, K. van der El, and M. M. van Paassen, "Manual Control Cybernetics: State-of-the-Art and Current Trends," *IEEE Transactions on Human-Machine Systems*, 2017.

[15] T. Melman, J. C. de Winter, and D. A. Abbink, "Does haptic steering guidance instigate speeding? A driving simulator study into causes and remedies," *Accident Analysis and Prevention*, vol. 98, pp. 372–387, 2017.

[16] F. Mars, M. Deroo, and C. Charron, "Driver adaptation to haptic shared control of the steering wheel," *Conference Proceedings - IEEE International Conference on Systems, Man and Cybernetics*, pp. 1505–1509, 2014.

[17] A. W. De Jonge, J. G. Wildenbeest, H. Boessenkool, and D. A. Abbink, "The Effect of Trial-by-Trial Adaptation on Conflicts in Haptic Shared Control for Free-Air Teleoperation Tasks," *IEEE Transactions on Haptics*, vol. 9, no. 1, pp. 111–120, 2016.

[18] S. Ikemoto, H. B. Amor, T. Minato, B. Jung, and H. Ishiguro, "Physical human-robot interaction: Mutual learning and adaptation," *IEEE Robotics and Automation Magazine*, vol. 19, no. 4, pp. 24–35, 2012.

[19] S. Nikolaidis, D. Hsu, and S. Srinivasa, "Human-robot mutual adaptation in collaborative tasks: Models and experiments," *The International Journal of Robotics Research*, vol. 36, no. 5-7, pp. 618–634, 2017.

[20] D. T. McRuer and H. R. Jex, "A Review of Quasi-Linear Pilot Models," *IEEE Transactions on Human Factors in Electronics*, vol. HFE-8, no. 3, pp. 231–249, 1967.

[21] P. Zaal, "Manual Control Adaptation to Changing Vehicle Dynamics in Roll–Pitch Control Tasks," *Journal of Guidance, Control, and Dynamics*, vol. 39, no. 5, pp. 1–13, 2016.

[22] E. R. Boer and R. V. Kenyon, "Estimation of Time Varying Delay Time in Non-Stationary Linear Systems: An Approach toMonitor Human Operator Adaptation in Manual Tracking Tasks," *IEEE Transactions on Systems Man and Cybernetics*, vol. 28, no. 1, pp. 89–99, 1998.

[23] A. Popovici, P. M. Zaal, and D. Pool, "Dual Extended Kalman Filter for the Identification of Time-Varying Human Manual Control Behavior," *AIAA Modeling and Simulation Technologies Conference*, p. 3666, 2017.

[24] A. Van Grootheest, D. M. Pool, M. van Paassen, and M. Mulder, "Identification of Time-Varying Manual Control Adaptations with Recursive ARX Models," *2018 AIAA Modeling and Simulation Technologies Conference*, no. January, pp. 1–22, 2018.

[25] D. T. McRuer, R. E. Magdaleno, and G. P. Moore, "A Neuromuscular Actuation System Model," *IEEE Transactions on Man-Machine Systems*, vol. 9, no. 3, pp. 61–71, 1968.

[26] J. R. Schiess and V. R. Roland, "Kalman filter estimation of human pilot-model parameters," *NASA TN D-8024*, no. November 1975, 1975.

[27] R. J. Kuiper, H. Boessenkool, J. C. L. Frumau, and D. A. Abbink, "A Haptic Backhoe Excavator Simulator : How to Reflect Natural Occurring Interaction Forces," *Manuscript submitted for publication*, 2018.

[28] H. J. Damveld, G. C. Beerens, M. M. Van Paassen, and M. Mulder, "Design of Forcing Functions for the Identification of Human Control Behavior," *Journal of Guidance, Control, and Dynamics*, vol. 33, no. 4, pp. 1064–1081, 2010.

[29] J. Bradley, "Complete Counterbalancing of Immediate Sequential Effects in a Latin Square," *Journal of the American Statistical Association*, vol. 53, no. 282, pp. 525–528, 1958.

[30] J. D. Van Der Laan, A. Heino, and D. De Waard, "A simple procedure for the assessment of acceptance of advanced transport telematics," *Transportation Research Part C: Emerging Technologies*, vol. 5, no. 1, pp. 1–10, 1997.

[31] S. S. Shapiro and M. B. Wilk, "An Analysis of Variance Test for Normality (Complete Samples)," *Biometrika*, vol. 52, no. 3/4, p. 591, 1965.

[32] J. Demšar, "Statistical Comparisons of Classifiers over Multiple Data Sets," *Journal of Machine Learning Research*, vol. 7, pp. 1–30, 2006.

[33] J. W. Mauchly, "Significance Test for Sphericity of a Normal n-Variate Distribution Author," *The Annals of Mathematical Statistics*, vol. 11, no. 2, pp. 204–209, 1940.

[34] S. W. Greenhouse and S. Geisser, "On methods in the analysis of profile data," *Psychometrika*, vol. 24, no. 2, pp. 95–112, 1959.

[35] J. M. Bland and D. G. Altman, "Multiple significance tests: the Bonferroni method," *BMJ*, vol. 310, p. 170, 1995.

[36] M. Friedman, "The Use of Ranks to Avoid the Assumption of Normality Implicit in the Analysis of Variance," *Journal of the American Statistical Association*, vol. 32, no. 200, pp. 675–701, 1937.

[37] F. Wilcoxon, "Individual Comparisons by Ranking Methods," *Biometrics Bulletin*, vol. 1, no. 6, pp. 80–83, 1945.

[38] B. Adams, E. C. Holmes, C. Zhang, M. P. Mammen, S. Nimmannitya, S. Kalayanarooj, and M. Boots, "Cross-protective immunity can account for the alternating epidemic pattern of dengue virus serotypes circulating in Bangkok," *Proceedings of the National Academy of Sciences*, vol. 103, no. 38, pp. 14 234–14 239, 2006.

[39] M. A. Goodrich, W. C. Stirling, and L. R. Bolr, "Satisficing revisited," *Minds and Machines*, vol. 10, no. 1, pp. 79–110, 2000.

[40] D. T. McRuer, "Remarks on some neuromuscular subsystem dynamics," *IEEE Transactions on Human Factors in Electronics*, vol. 7, no. 3, pp. 129–130, 1966.

[41] D. M. Pool, G. A. Harder, and M. M. van Paassen, "Effects of Simulator Motion Feedback on Training of Skill-Based Control Behavior," *Journal of Guidance, Control, and Dynamics*, vol. 39, no. 4, pp. 889–902, 2016.

[42] H. E. Rauch, F. Tung, and C. T. Striebel, "Maximum likelihood estimates of linear dynamic systems," *AIAA Journal*, vol. 3, no. 8, pp. 1445–1450, 1965.

[43] L. Loron and G. Laliberté, "Application of the extended Kalman filter to parameters estimation of induction motors," *Fifth European Conference on Power Electronics and Applications*, pp. 85–90, 1993.

APPENDIX A
EXPERIMENTAL BRIEFING

Experiment Briefing

Adaptive Haptic Shared Control

Thank you for your contribution to this scientific endeavour! You will be participating in a tracking experiment in the Human-Robot Interaction Laboratory (HRILab) at TU Delft, in which the effect of adaptive haptic shared control is studied. This briefing will introduce you to the experiment and what is expected of you as a participant.

Experiment Goal

The goal of this experiment is to investigate the effect of several types of guidance forces (haptic shared control). The objective is to find a haptic shared controller that assists the human without causing annoying conflicts.

Tracking Task

The task you will carry out is a tracking task using a so called "compensatory display". In this task, it is **your goal to minimize the error shown on the screen**. The error between the desired and current position is displayed on a display by a moving horizontal blue line. The desired position is shown as an orange line on the centre of the screen. Control inputs (in a forward/backward direction) can be given using the joystick. The experimental set-up is shown in the picture. In this case, the blue line is lower than the orange reference line and the joystick should be pushed forward to reduce the error.

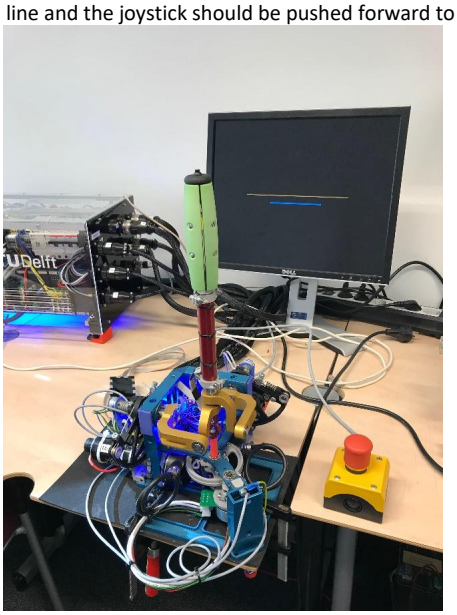

Each run starts with controlling the velocity of the blue line. This means that the blue line has a constant speed if the joystick remains in a single position. During the run, this will change and you will control the acceleration of the blue line. This means that the blue line has a constant acceleration if the joystick remains in a single position. At the end of the run, you will again control the velocity of the blue line. Those changes occur unannounced.

The joystick

In some conditions, the joystick will be exerting assistive forces. The forces are limited to 4 Newton, this means that you are always able to override the assistive forces. It is however, important to hold the joystick firmly in a fist. **If, for any reason, you want to stop the experiment during the execution of a task, please use the emergency button to stop the joystick.** After this, the joystick can be safely released.

To hold the joystick, please hold the handle with your thumb and index finger at the position of the upper screws. Your other fingers can be placed around the handle. **There is no need to squeeze the handle, however, it should be firmly connected to your hand.** The picture underneath shows how you should hold the joystick.

Experiment Procedures

Four different conditions will be assessed during the experiment. The experiment is divided into four sessions of four runs. Every experimental run takes approximately 3 minutes. After two sessions, there is a short break.

Before the first session, a couple of training runs are performed to let you get familiar with the task. First you will perform training runs for velocity control, after that you will perform training runs for acceleration control. The training session ends with performing the complete task. The other four sessions will consist of four runs with different haptic shared controllers. Your objective in every run is to minimize the error between the blue and orange line. After every run, the experimenter will tell you your achieved performance by giving the “root mean square error” (a measure for the mean error) of the last run. The lower this value, the better your performance. Please note that the experimental conditions also influence your performance, so the performance may vary between different conditions.

After every run, you are asked to subjectively rate this condition. You are asked to score nine items, regarding the satisfaction and usefulness of the condition.

Note on haptic shared control

During some of the conditions, you will receive guidance from a haptic shared controller. This guidance may or may not be correct and useful. It is important to remember that **your objective is to minimize the error shown on the screen, regardless of the guidance** you are given by the haptic shared controller.

Experiment Execution

For each tracking run, the subsequent procedure will be followed:

1. The researcher applies the settings for the next run.
2. The researcher checks whether the participant is ready to proceed and initiates the run after a countdown from 3 (3-2-1-go).
3. The participant performs the tracking task.
4. The participant can release the joystick when the black screen disappears.
5. The researcher asks the participant to assess the condition
6. The researcher informs the participant of the performance in the completed run

In total, the experiment will take approximately two hours.

Contact information researcher:	Contact information research supervisor	Contact information research supervisor
Jacco Vos	dr. ir. David Abbink	dr. ir. Daan Pool
jacco.e.vos@hotmail.com	d.a.abbink@tudelft.nl	d.m.pool@tudelft.nl
+31 6 219 00 845		

APPENDIX B
CONSENT FORM

Experiment Consent Form

Adaptive Haptic Shared Control

I hereby confirm that:

1. I volunteer to participate in the experiment conducted by the researcher (**Jacco Vos**) under Supervision of **dr.ir. David Abbink** from the Faculty of 3mE of TU Delft and **dr.ir. Daan Pool** from the Faculty of Aerospace Engineering of TU Delft. I understand that my participation in this experiment is voluntary and that I may withdraw and discontinue participation at any time, for any reason.
2. I have read the experiment briefing. Also, I affirm that I understand the experiment instructions and have had all remaining questions answered to my satisfaction.
3. I understand that my participation involves performing a simple control task that involves conditions where haptic shared control is present. Also, I understand the researcher will request subjective assessments from me throughout the experiment.
4. I confirm that the researcher has provided me with detailed safety and operational instructions for the hardware used in the experiment.
5. I understand that the researcher will not identify me by name in any reports or publications that will result from this experiment, and that my confidentiality as a participant in this study will remain secure.
6. I understand that this research study has been reviewed and approved by the TU Delft Human Research Ethics Committee (HREC). To report any problems regarding my participation in the experiment, I know I can contact the researchers using the contact information below or, if necessary, the TU Delft HREC (hrec@tudelft.nl).
7. I have been given a copy of this consent form.

My Signature	Date
My Name	Signature of researcher

Contact information researcher:	Contact information research supervisor	Contact information research supervisor
Jacco Vos	dr. ir. David Abbink	dr. ir. Daan Pool
jacco.e.vos@hotmail.com	d.a.abbink@tudelft.nl	d.m.pool@tudelft.nl
+31 6 219 00 845		

APPENDIX C
GENERAL QUESTIONNAIRE

Questionnaire: General information

Adaptive Haptic Shared Control

Participant number:	
Date:	
Age:	
Left/righthandedness:	L / R
Gender:	F / M
Do you where glasses or contacts?	No / Yes, …
Do you suffer from colour blindness?	No / Yes, …
I have good steering/ manoeuvring/pointing skills in video games (1 = completely disagree, 10 = completely agree)	1 / 2 / 3 / 4 / 5 / 6 / 7 / 8 / 9 / 10
Can you describe any previous experience with tracking tasks?	None / …

APPENDIX D
HUMAN RESEARCH ETHICS APPROVAL

Date 07-02-2018
Contact person Ir. J.B.J. Groot Kormelink, secretary HREC
Telephone +31 152783260
E-mail j.b.j.grootkormelink@tudelft.nl

Human Research Ethics Committee
TU Delft
(http://hrec.tudelft.nl/)

Visiting address
Jaffalaan 5 (building 31)
2628 BX Delft

Postal address
P.O. Box 5015 2600 GA Delft
The Netherlands

Ethics Approval Application: Co-adaptive Haptic Shared Control
Applicant: Petermeijer, Bastiaan

Dear Bastiaan Petermeijer,

It is a pleasure to inform you that your application mentioned above has been approved.

Good luck with your research!

Sincerely,

Prof. Dr. Sabine Roeser
Chair Human Research Ethics Committee TU Delft

Prof.dr. Sabine Roeser
TU Delft
Head of the Ethics and Philosophy of Technology Section
Department of Values, Technology, and Innovation
Faculty of Technology, Policy and Management
Jaffalaan 5
2628 BX Delft
The Netherlands
+31 (0) 15 2788779
S.Roeser@tudelft.nl
www.tbm.tudelft.nl/sroeser

APPENDIX E
EXTENDED KALMAN FILTER

The pilot model from Equation 2 can be rewritten into state space form. This results in the equations below.

$$\dot{x}(t) = \begin{bmatrix} -2\zeta_{nms}\omega_{nms} & 1 \\ -\omega_{nms}^2 & 0 \end{bmatrix} x(t) + \begin{bmatrix} K_{dot}\omega_{nms}^2 K + K_e\omega_{nms}^2 B - 2\zeta_{nms}K_{dot}\omega_{nms}^3 B \\ K_e\omega_{nms}^2 K - K_{dot}\omega_{nms}^4 B \end{bmatrix} e(t-\tau) \tag{8}$$

$$F(t) = \begin{bmatrix} 1 & 0 \end{bmatrix} x(t) + \begin{bmatrix} K_{dot}\omega_{nms}^2 B \end{bmatrix} e(t-\tau) \tag{9}$$

Combined estmation of the state $x(t)$ and the parameters of this linear model, leads to a non-linear estimation problem. Therefore, an Extended Kalman Filter (EKF) is used. The EKF in this paper is based on [43].

The first step is to discretize the state space model, as the EKF is a discrete estimator. A time step of δt is used.

$$t(k) = k \cdot \delta t \tag{10}$$

$$A_{d_{temp}}(k) = \sum_{n=1}^{6} \frac{(A(t(k))\delta t)^{n-1}}{(n-1)!} \tag{11}$$

$$B_{d_{temp}}(k) = \delta t \sum_{n=1}^{6} \frac{(A(t(k))\delta t)^{n-2}}{(n-1)!} B(t(k)) \tag{12}$$

$$C_{d_{temp}}(k) = C(t(k)) \tag{13}$$

$$D_{d_{temp}}(k) = D(t(k)) \tag{14}$$

$$\tag{15}$$

For this implementation of the EKF, the discrete D matrix should be equal to 0. Therefore, an additional state is introduced. The additional state is the predicted output.

$$A_d(k) = \begin{bmatrix} A_{d_{temp}}(k) & \emptyset \\ C_{d_{temp}}(k) & \emptyset \end{bmatrix} \tag{16}$$

$$B_d(k) = \begin{bmatrix} B_{d_{temp}}(k) \\ D_{d_{temp}}(k) \end{bmatrix} \tag{17}$$

$$C_d(k) = \begin{bmatrix} \emptyset & 1 \end{bmatrix} \tag{18}$$

$$D_d(k) = 0 \tag{19}$$

This discrete state space model can now be used for simultaneous estimation of the parameters of the state using the EKF. During every time step, the following computations are executed.

The first step is the prediction step where parameters θ and discrete state ϕ are predicted.

$$\phi(k+1|k) = A_d(k)\phi(k|k) + B_d(k)e(k-\tau_d) \tag{20}$$

$$\theta(k+1|k) = \theta(k|k) \tag{21}$$

Now, the augmented model (where the state is augmented with the parameters) is linearized using the parameters of the previous time step.

$$F(k) = \begin{bmatrix} A_d(k) & \frac{\partial A_d(k)\phi(k|k) + B_d(k)e(k-\tau_d)}{\partial \theta(k|k)} \\ \emptyset & \mathrm{I} \end{bmatrix} \tag{22}$$

$$H(k) = \begin{bmatrix} C_d(k) & \emptyset \end{bmatrix} \tag{23}$$

The next step is the prediction of the covariance matrix.

$$P(k+1|k) = F(k)P(k|k)F^T(k) + Q \tag{24}$$

And finally a correction is performed using Kalman gain $K(k+1)$.

$$K(k+1) = \frac{P(k+1|k)H^T(k)}{H(k)P(k+1|k)H^T(k) + R} \tag{25}$$

$$P(k+1|k+1) = \left(\mathrm{I} + K(k+1)H(k)\right) P(k+1|k) \tag{26}$$

$$\begin{bmatrix} \phi(k+1|k+1) \\ \theta(k+1|k+1) \end{bmatrix} = \begin{bmatrix} \phi(k+1|k) \\ \theta(k+1|k) \end{bmatrix} + K(k+1)\left(F(k+1) - H(k)\phi(k+1|k)\right) \tag{27}$$

The settings of the EKF that can be tuned are the initial covariance matrix $P(t=0)$, the measurement noise covariance R and the state noise covariance matrix Q. Those settings were tuned based on the prestudy data (see Appendix G). The resulting settings are displayed below.

$$P(t=0) = \begin{bmatrix} 1 & 0 & 0 & 0 & 0 & 0 & 0 \\ 0 & 1 & 0 & 0 & 0 & 0 & 0 \\ 0 & 0 & 1 & 0 & 0 & 0 & 0 \\ 0 & 0 & 0 & 1 & 0 & 0 & 0 \\ 0 & 0 & 0 & 0 & 1 & 0 & 0 \\ 0 & 0 & 0 & 0 & 0 & 1 & 0 \\ 0 & 0 & 0 & 0 & 0 & 0 & 1 \end{bmatrix} \tag{28}$$

$$Q = \begin{bmatrix} 10^{-8} & 0 & 0 & 0 & 0 & 0 & 0 \\ 0 & 10^{-8} & 0 & 0 & 0 & 0 & 0 \\ 0 & 0 & 10^{-8} & 0 & 0 & 0 & 0 \\ 0 & 0 & 0 & 10^{-7} & 0 & 0 & 0 \\ 0 & 0 & 0 & 0 & 10^{-6} & 0 & 0 \\ 0 & 0 & 0 & 0 & 0 & 10^{-6} & 0 \\ 0 & 0 & 0 & 0 & 0 & 0 & 10^{-7} \end{bmatrix} \tag{29}$$

$$R = 5 \tag{30}$$

$$\phi(t=0) = \begin{bmatrix} 0 \\ 0 \\ 0 \end{bmatrix} \tag{31}$$

$$\theta(t=0) = \begin{bmatrix} K_{dot}(t=0) \\ K_e(t=0) \\ \omega_{nms}(t=0) \\ \zeta_{nms}(t=0) \end{bmatrix} = \begin{bmatrix} 0 \\ 1.5 \\ 8 \\ 0.3 \end{bmatrix} \tag{32}$$

APPENDIX F
SIMULATION RESULTS

A simulation is performed to be able to compare the identified parameters with the actual parameters. This way, a conclusion can be drawn on the accuracy of the parameter estimation scheme.

The identified time-varying parameters from the prestudy are used to model the human (see Table IV). Remnant is modeled as colored noise with a power of 25% of the human force [21]. The EKF is now used to identify the parameters and reproduce the force. In Figure 10, the simulated and reproduced force are shown, together with the innovation and innovation covariance [23]. The EKF is able to reproduce the simulated force almost perfectly, resulting in a VAF of 92.0 %. It can also be seen that the innovation is well within the bound set by the innovation covariance.

The estimated parameters are shown in Figure 11. The estimated gains closely resemble the actual gains, with a settling time of approximately 15 seconds after a step change. The neuromuscular parameters, however, are more difficult to estimate. A bias is present for the neuromuscular frequency and a long settling time van be seen for the neuromuscular damping.

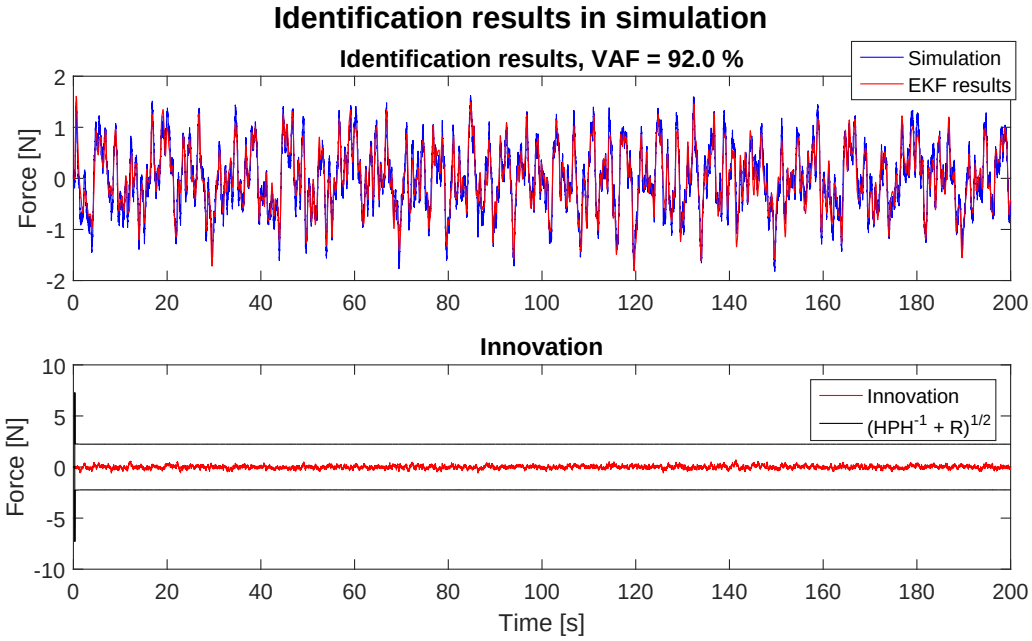

Fig. 10: Simulation results of human force, expected force, innovation and innovation covariance

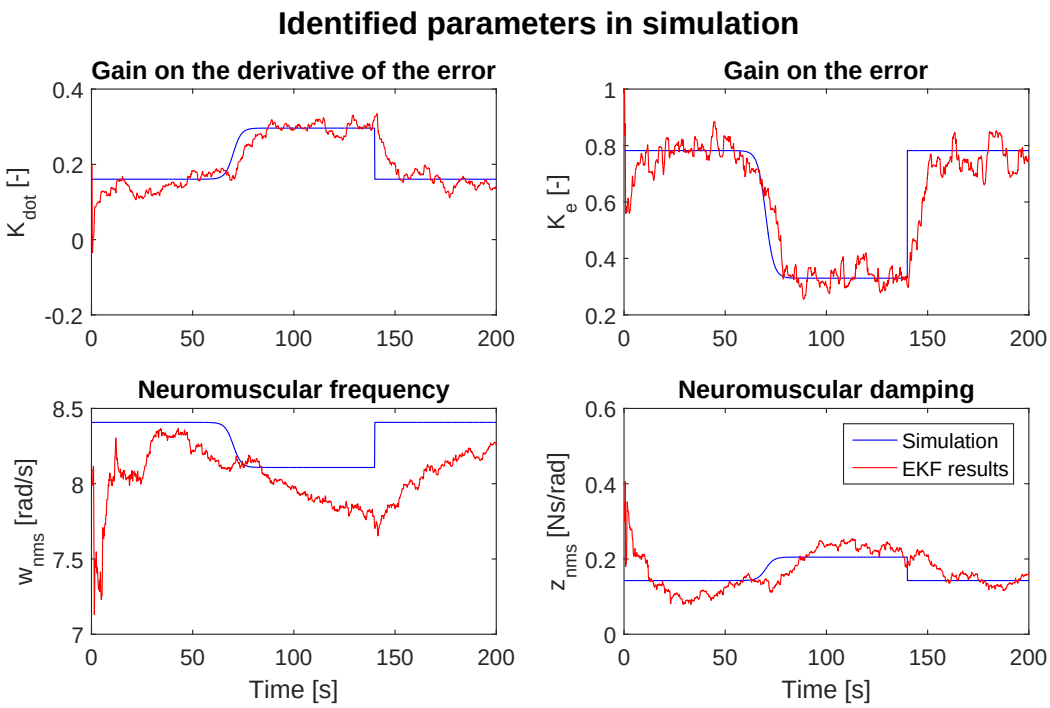

Fig. 11: Simulation results of estimated parameters

APPENDIX G
ESTIMATION RESULTS DURING THE PRESTUDY

For estimation the parameters for the controller, a prestudy was conducted with four subjects. Those four subjects performed manual control trials until the performance did no longer improve (RMSE did no longer decrease). Using the last trial from every participant, average FRFs were calculated for controlling a single integrator (segments 1 and 5) and controlling a double integrator (segment 3).

First, the average FRF of the joystick was calculated based on segments 1, 3, and 5. The resulting FRF and fitted model are shown in Figure 14. The coherence of the joystick is very high, indicating that the joystick can be accurately described by a linear model. The model is able to fit both the magnitude and phase, indicating that the mass of the joystick can indeed be neglected.

The next step was computing the FRFs of the human during control of a single integrator (see Figure 12) and during control of a double integrator (see Figure 13). The model from Equation 2 was fitted, using the joystick parameters that were already identified. It can be seen that the model accurately follows both the magnitude and the phase of the human FRFs, expect for the low frequencies in segment 3. This can be explained by the fact that the signal-to-noise ratio at those frequencies is low. The human gain for low frequencies is very low, resulting in a low signal-to-noise ratio. This is also indicated by the low coherence at those frequencies.

The identified parameters are used for the time-invariant and *a priori* optimized HSC. For time-invariant HSC, the identified parameters for segments 1 and 5 are used during the entire trial. For *a priori* optimized HSC, the scheduling function of the controlled element dynamics is used, with the identified parameters for controlling a single and a double integrator. The HSC parameters are listed in Table IV. Note that the gains are multiplied with 0.5, to make sure the HSC delivers half the required force. A factor of 0.5 was chosen, because this corresponds to co-adaptive HSC, where the controller and human both exert half the force.

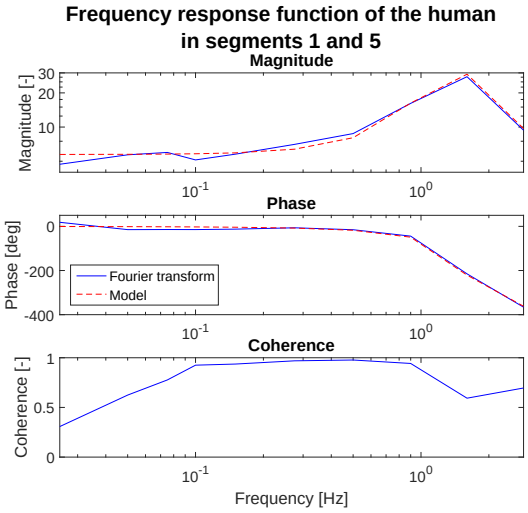

Fig. 12: Pilot model for the human during control of a single integrator during the prestudy.

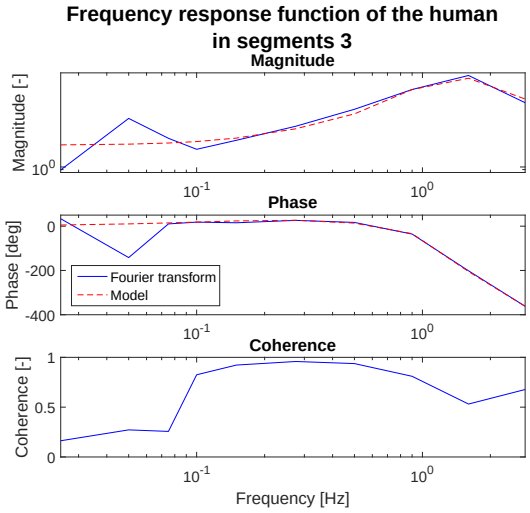

Fig. 13: Pilot model for the human during control of a double integrator during the prestudy.

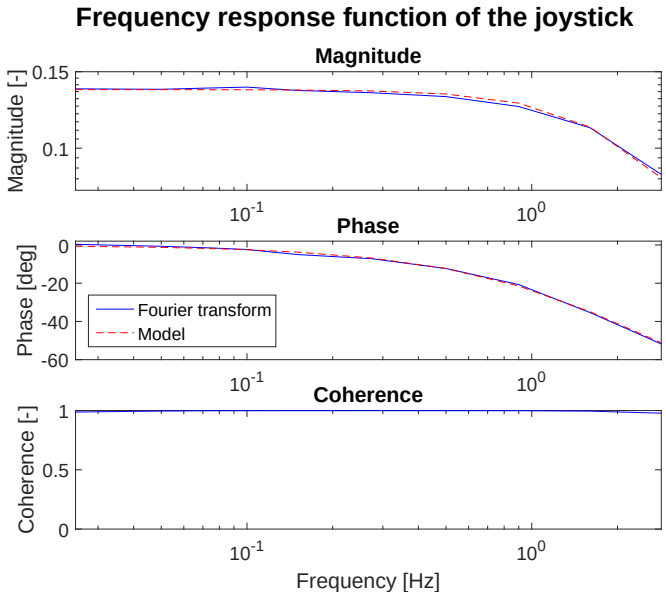

Fig. 14: Joystick model during the prestudy.

TABLE IV: Parameters for time-invariant HSC and *a priori* optimized HSC based on an average response of four subjects in a prestudy. Note that the gains are multiplied by 0.5, so the HSC delivers half the required force.

HSC type	Time-invariant	*A priori* optimized		
Segment	1-5	1	3	5
K_{dot} [-]	0.1605	0.1605	0.2962	0.1605
K_e [-]	0.7821	0.7821	0.3300	0.7821
τ [s]	0.3096	0.3096	0.3242	0.3096
ω_{nms} [rad/s]	8.4073	8.4073	8.1079	8.4073
ζ_{nms} [Ns/rad]	0.1427	0.1427	0.2049	0.1427
B [Ns/rad]	0.5089	0.5089	0.5089	0.5089
K [N/rad]	7.3302	7.3302	7.3302	7.3302

APPENDIX H
OFFLINE ESTIMATION DURING THE EXPERIMENT

During the training phase of the experiment, the joystick parameters are estimated. An average frequency response function of the joystick is calculated during state state segments (segments 1, 3, and 5). In the frequency domain, the joystick parameters (B and K) are estimated using the `lsqnonlin`-command from the optimization toolbox in Matlab. Secondly, the average frequency response function of the operator is calculated based on segments 1 and 5 to estimate the time delay (τ). The fits of the joystick model in frequency domain are shown in Figures 15 to 25.

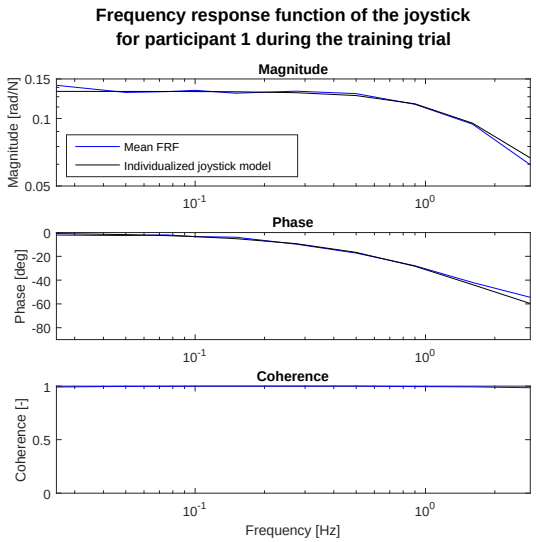

Fig. 15: Joystick model for participant 1

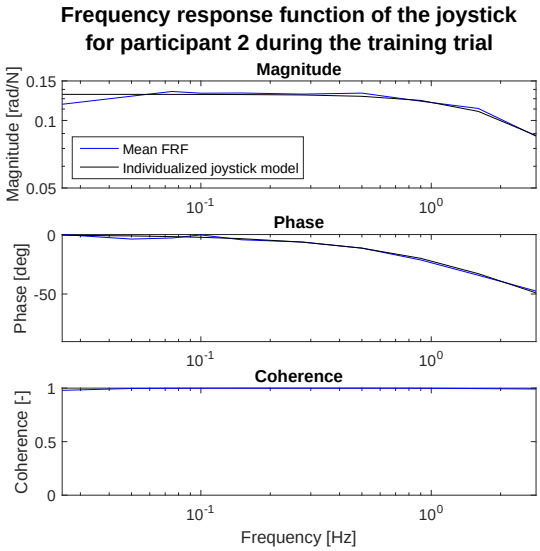

Fig. 16: Joystick model for participant 2

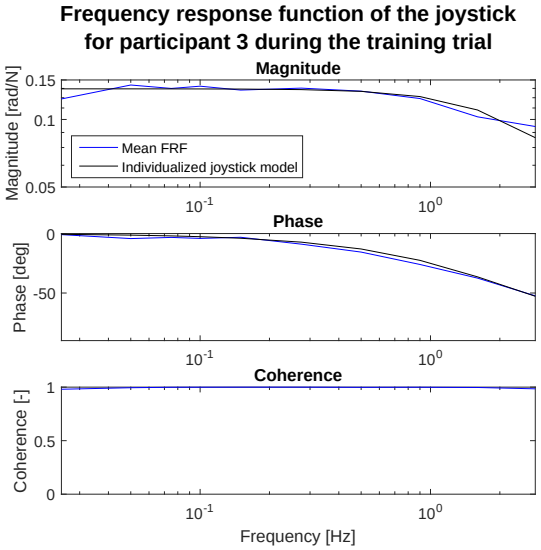

Fig. 17: Joystick model for participant 3

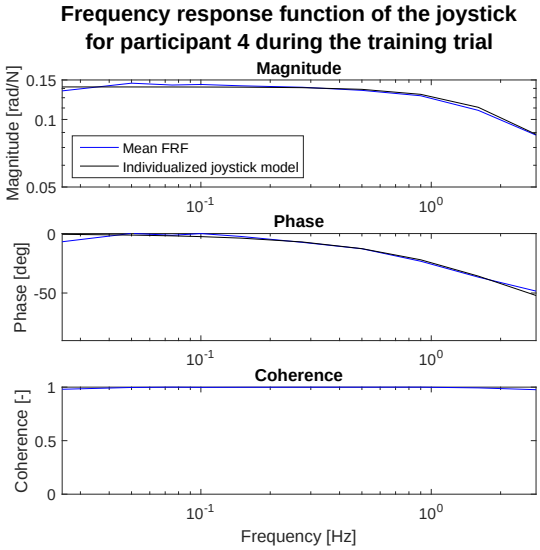

Fig. 18: Joystick model for participant 4

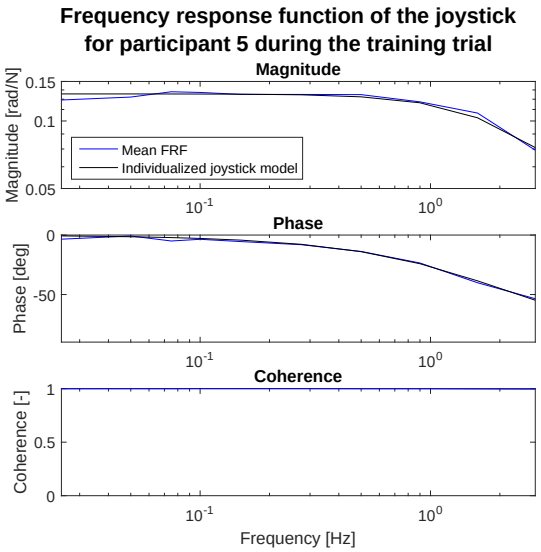

Fig. 19: Joystick model for participant 5

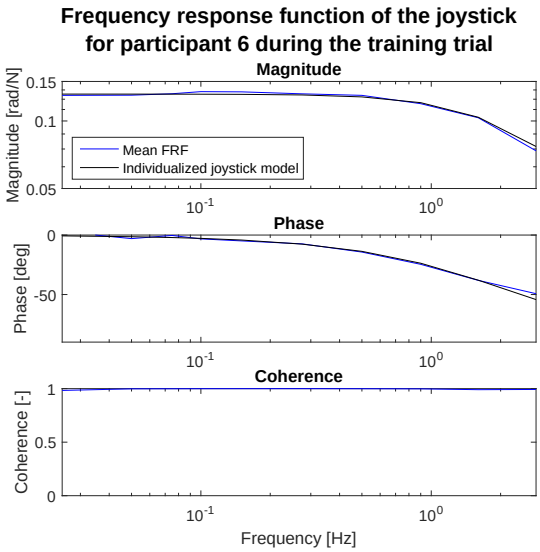

Fig. 20: Joystick model for participant 6

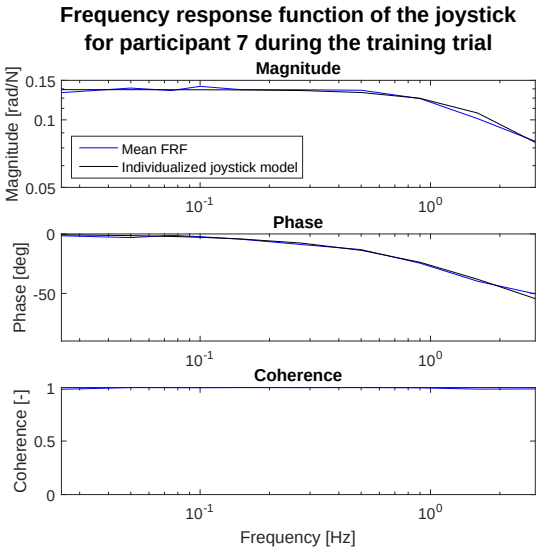

Fig. 21: Joystick model for participant 7

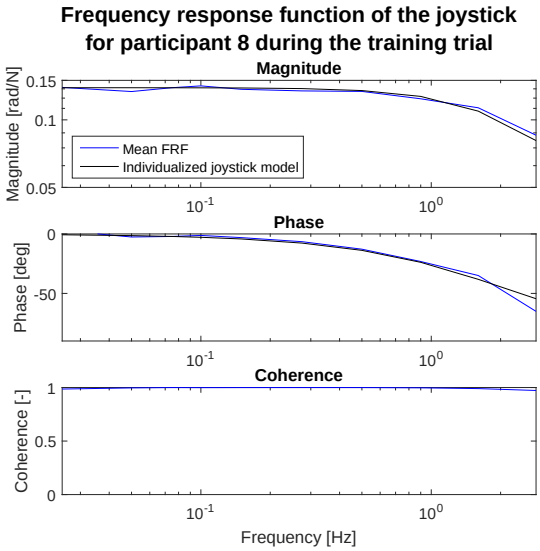

Fig. 22: Joystick model for participant 8

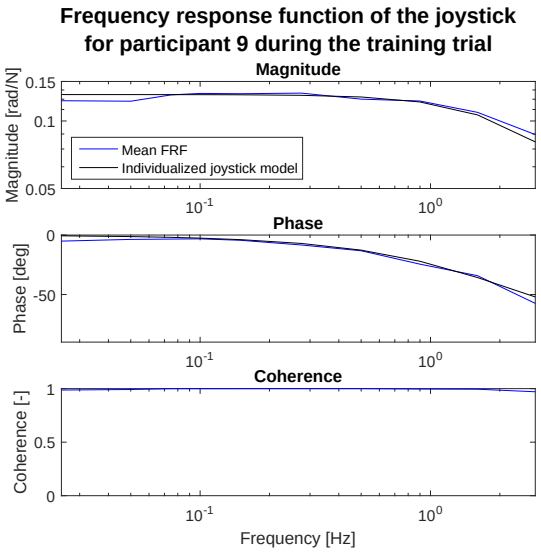

Fig. 23: Joystick model for participant 9

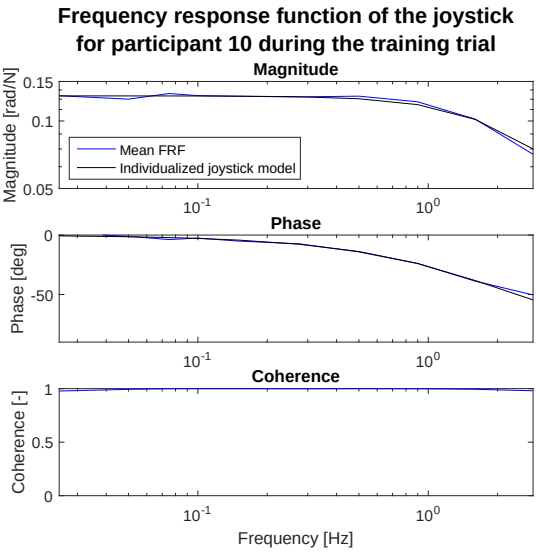

Fig. 24: Joystick model for participant 10

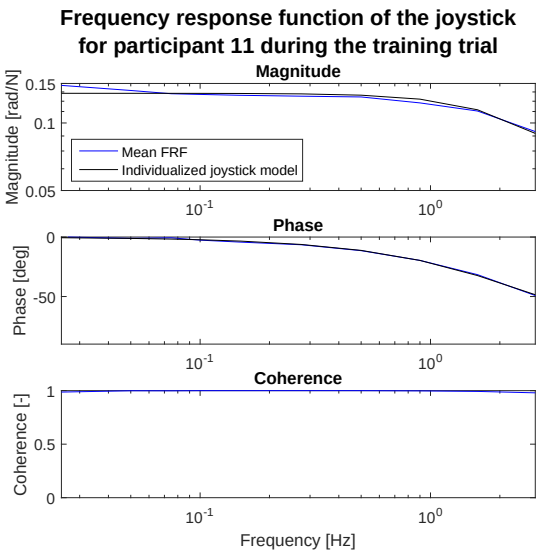

Fig. 25: Joystick model for participant 11

APPENDIX I
ONLINE ESTIMATION DURING THE EXPERIMENT

The EKF estimated four parameters (K_{dot}, K_e, ω_{nms}, and ζ_{nms}) online during every trial. The mean estimated parameters (averaged over participants and trials) per condition are shown in Figure 26 for every segment. The average variance of the estimated parameter during each segment is shown in Figure 27.

Both gains (K_{dot} and K_e) are generally lower for all HSC conditions compared to manual control. In segment 3, K_e is significantly lower for time-invariant HSC compared to *a priori* optimized HSC and co-adaptive HSC. In this condition, the K_e of the haptic shared controller is so high that the human gain on the error is sometimes even negative. No significant differences are seen in average neuromuscular damping. The neuromuscular frequency, however, is significantly lower for HSC conditions compared to manual control. In the simulation results (Appendix F), it was seen that a bias was present for the neuromuscular frequency. A possible explanation could be that this bias increases for HSC trials.

Compared to manual control, both gains are estimated to be lower during co-adaptive HSC while the neuromuscular parameters are approximately equal. This indicates that the estimated parameters are reasonable. The low VAF during co-adaptive HSC conditions (see Figure 4) cannot (fully) be explained by incorrectly estimated parameters. The fact that the human also reacts to HSC force, however, is a plausible explanation, because this dependency cannot be represented by the model.

In general, no significant differences exist for the variance of the estimated parameters. However, for the neuromuscular damping, it can be seen that during control of a double integrator (segments 2b and 3) the variance of the neuromuscular damping is higher (significantly so in segment 3, and only for some participants in segment 2b). This is also reflected by the fact that the neuromuscular parameters are estimated very low or even negative for some trials. This problem is further discussed in Appendix L.

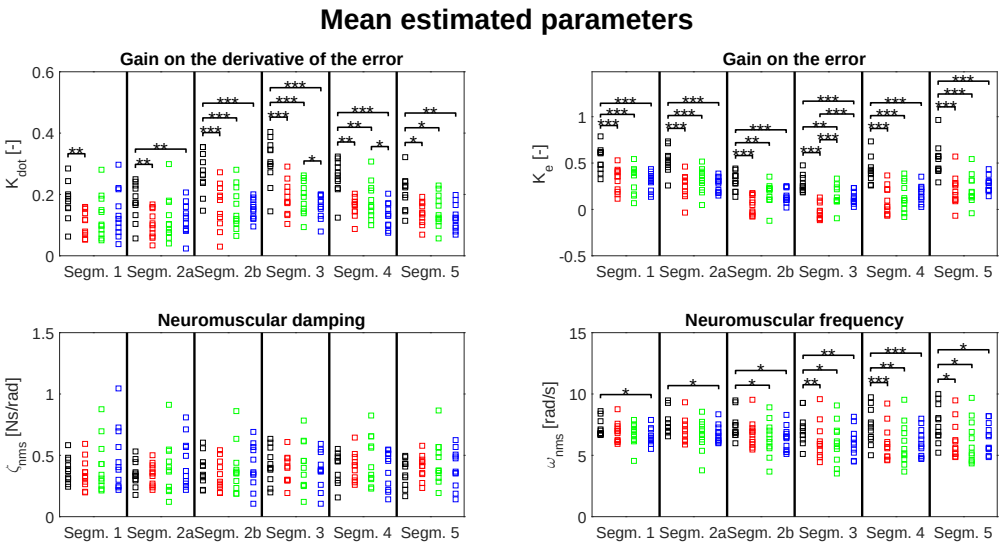

Fig. 26: Mean estimated parameters per segment for the four conditions, data points represent participant's means. The stars represent significance, one star means $p \leq 0.05$, two stars mean $p \leq 0.01$, and three stars mean $p \leq 0.001$.

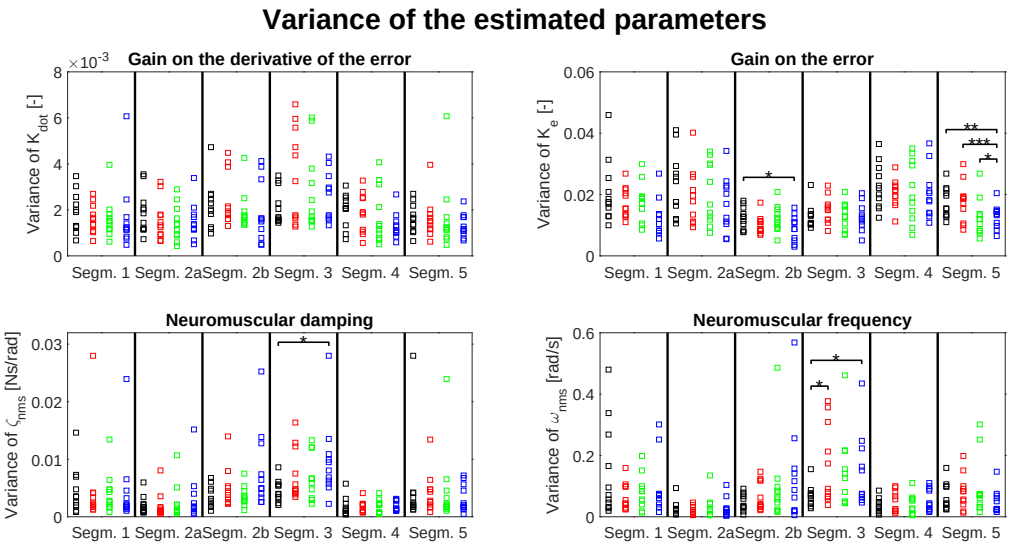

Fig. 27: Variance of the estimated parameters during each segment for the four conditions, data points represent participant's means. The stars represent significance, one star means $p \leq 0.05$, two stars mean $p \leq 0.01$, and three stars mean $p \leq 0.001$.

APPENDIX J
JOYSTICK FRF DURING MANUAL CONTROL AND CO-ADAPTIVE HSC

The joystick is modeled as an open loop system that has a force as the input and the joystick angle as the output. However, in reality, a closed loop system is present, including the grip dynamics [14], [40]. To study the influence of the grip dynamics, joystick FRFs are computed both during manual control trials and co-adaptive HSC trials. I the grip dynamics have a large influence, it is expected that there is a difference between manual control trials and co-adaptive HSC trials, as the shared control forces have an influence as well.

In Figure 28, the mean joystick FRF for all participants is shown for manual control and co-adaptive HSC. It can be seen that the joystick frequency response is approximately equal. Therefore, it is concluded that the open loop approximation is also valid during HSC trials.

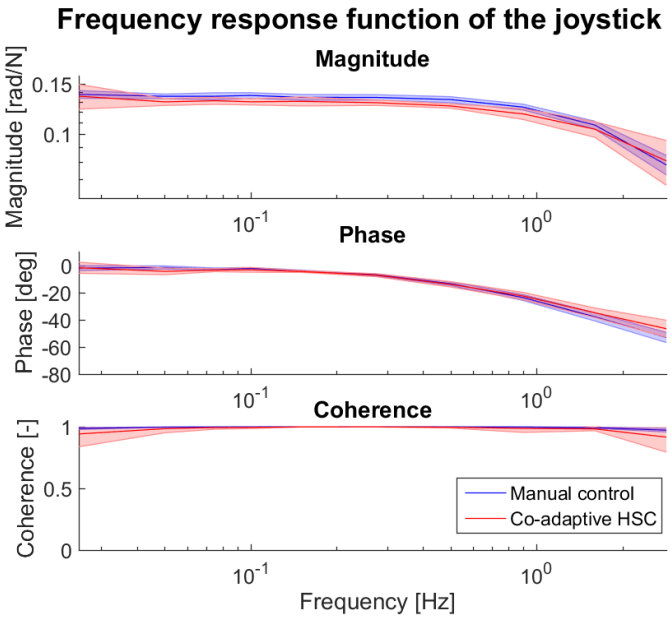

Fig. 28: Mean FRF of the joystick during manual control and co-adaptive HSC. The shaded areas represent the standard deviation over participants.

APPENDIX K
LEARNING EFFECTS

Because the order of the conditions is the same for all participants, learning effects can be present. In Figure 29, the learning effects are depicted. The mean values of the metrics, averaged over participants, are shown for every repetition. The order of the conditions in the first block is: time-invariant HSC, co-adaptive HSC, *a priori* optimized HSC, and manual control.

The performance of time-invariant HSC and co-adaptive HSC for the first repetition is substantially worse than the performance in the other repetitions. This indicates a learning effect is present. The same effect can be seen for control activity (although to a smaller extend) and control effort.

However, for the conflict rate, no learning effect is present. As the conflict rate was the metric of interest in this study, learning effects do not seem to have an effect on the conclusions drawn in this study. However, for future studies it is advised to balance the conditions across participants to cancel out any learning effects.

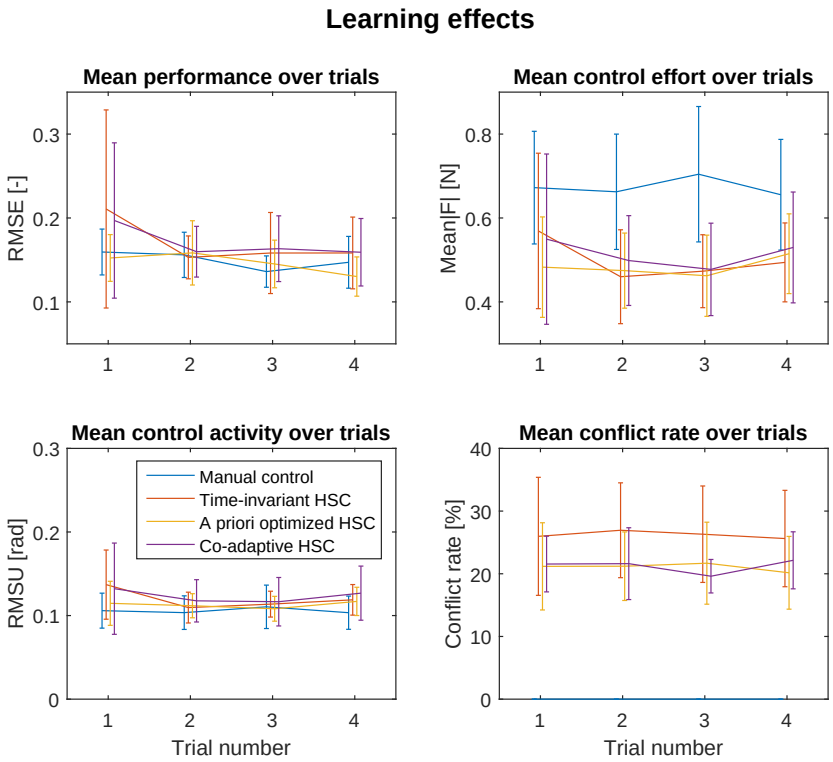

Fig. 29: Learning effects over the trials. Mean metrics are shown for each trial with error bars representing the standard deviation over participants.

APPENDIX L
OUT-OF-PHASE FORCE OSCILLATIONS

To detect out-of-phase force oscillation, the sliding window cross-correlation at lag $t = 0$ is used. If the cross-correlation is negative, the human force and HSC force are out-of-phase. For a sliding window of 10 seconds (with a sampling frequency of 100 Hz) a threshold of -5 is used, to increase the robustness of the indicator for out-of-phase force oscillations.

In Figure 30, the correlation between the negative damping rate and negative cross-correlation rate is shown. It can be seen that a high correlation exists (Peason's $\rho = 0.877$). For every trial where out-of-phase oscillations are present, the damping is estimated to be negative for some amount of time. This is another indication that the negative estimated damping causes the out-of-phase force oscillations.

The oscillation rate during all segments is shown for every condition in Figure 31. The non-zero oscillation rate for participant 9 for time-invariant HSC is caused by the fact that the blue line (representing the error) hits the top and the bottom of the screen, so this is not the same phenomenon. Out-of-phase force oscillations only occur for co-adaptive HSC. The oscillations are not present in the first two segments, but only after a transition of the controlled element. Especially in segment 4, right after a step change of the controlled element dynamics, the oscillations are present. This might indicate that the proposed estimation scheme is not able to track quickly changing parameters. The effect of the estimation (and adaptation) speed are subject to future work.

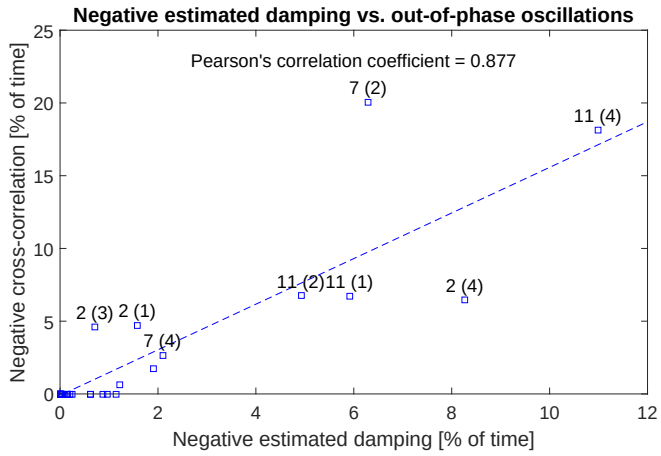

Fig. 30: A strong correlation exists between the percentage of the total time of the trial during which the damping was estimated to be a negative number and the percentage during which the windowed cross-correlation was negative (i.e. out-of-phase oscillations of control force are present). For some data points that show considerable out-of-phase oscillations, the participant number and the repetition number (between brackets) are shown.

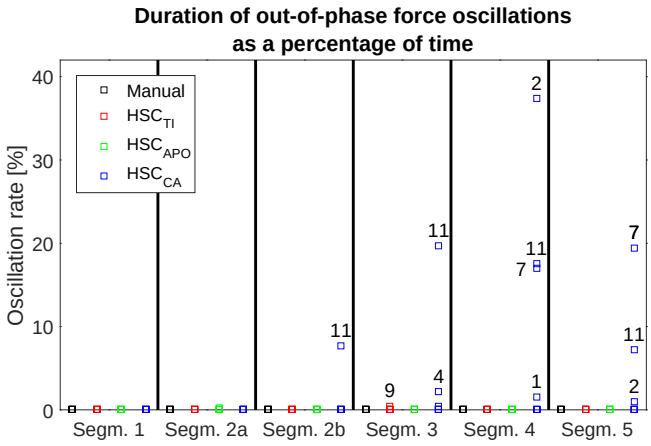

Fig. 31: Oscillation rate for all conditions in all segments. The participant numbers are shown for all data points that are not equal to zero.

APPENDIX M
INDIVIDUAL RESULTS FOR MANUAL CONTROL AND CO-ADAPTIVE HSC

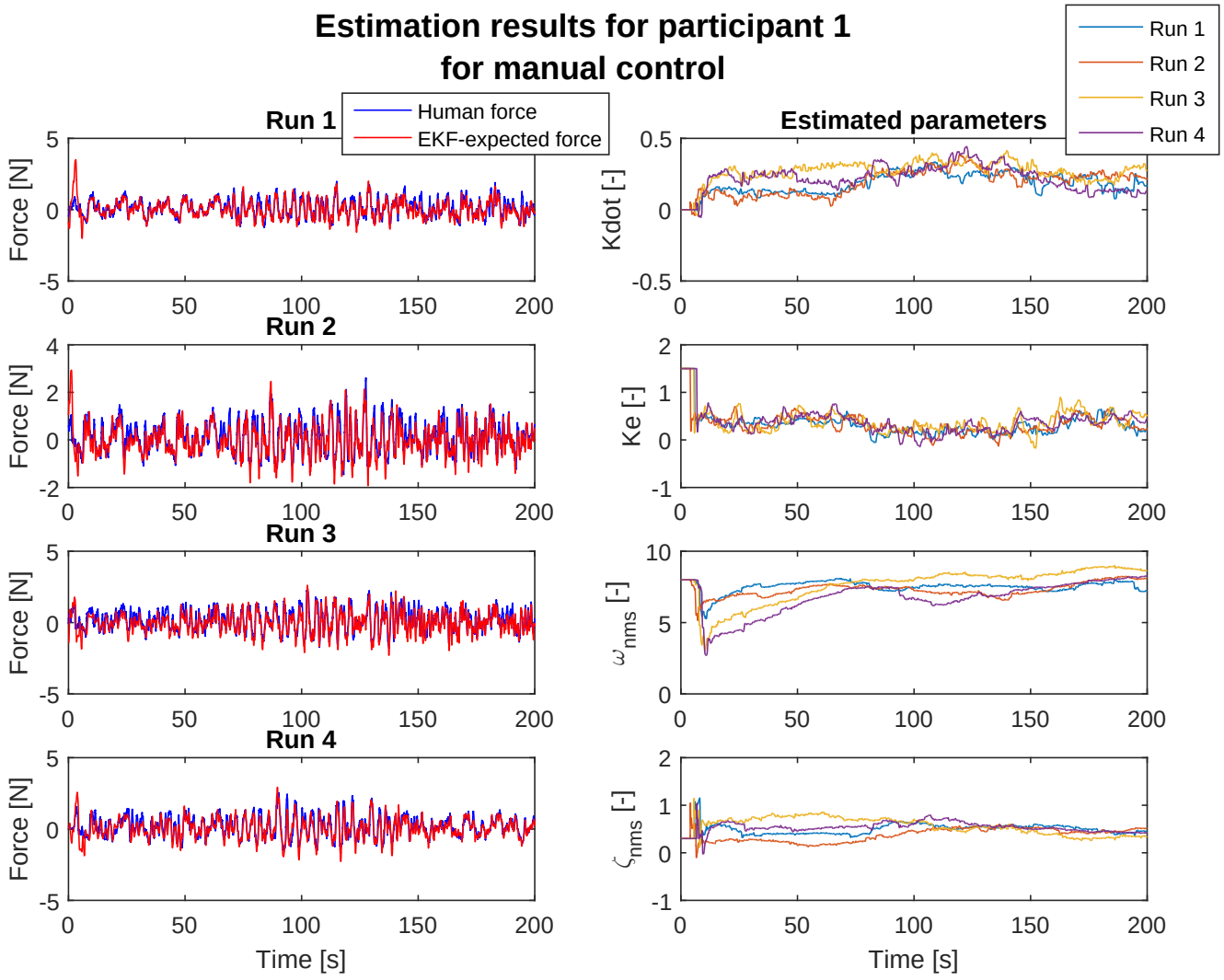

Fig. 32: Identification results participant 1, manual control

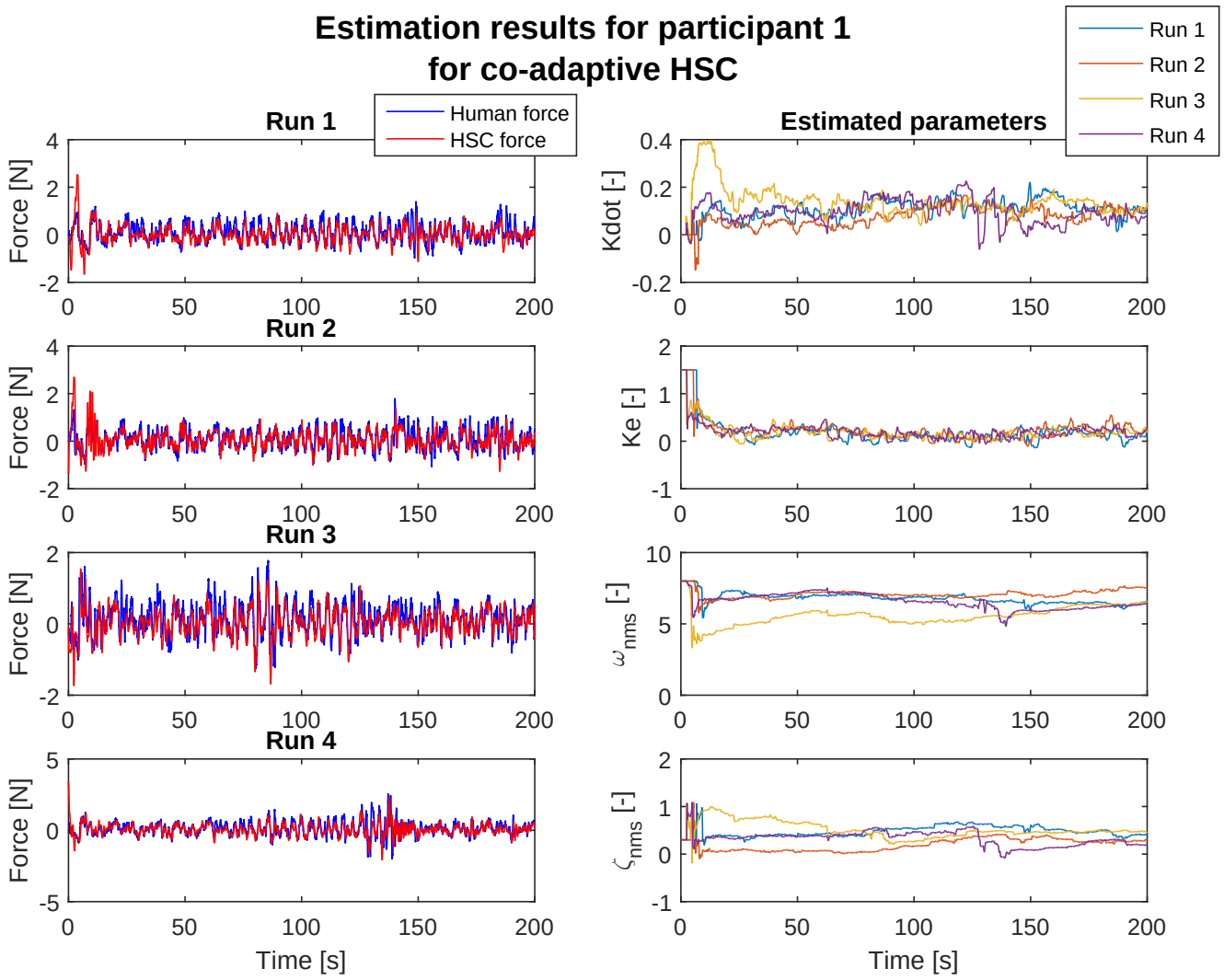

Fig. 33: Identification results participant 1, co-adaptive HSC

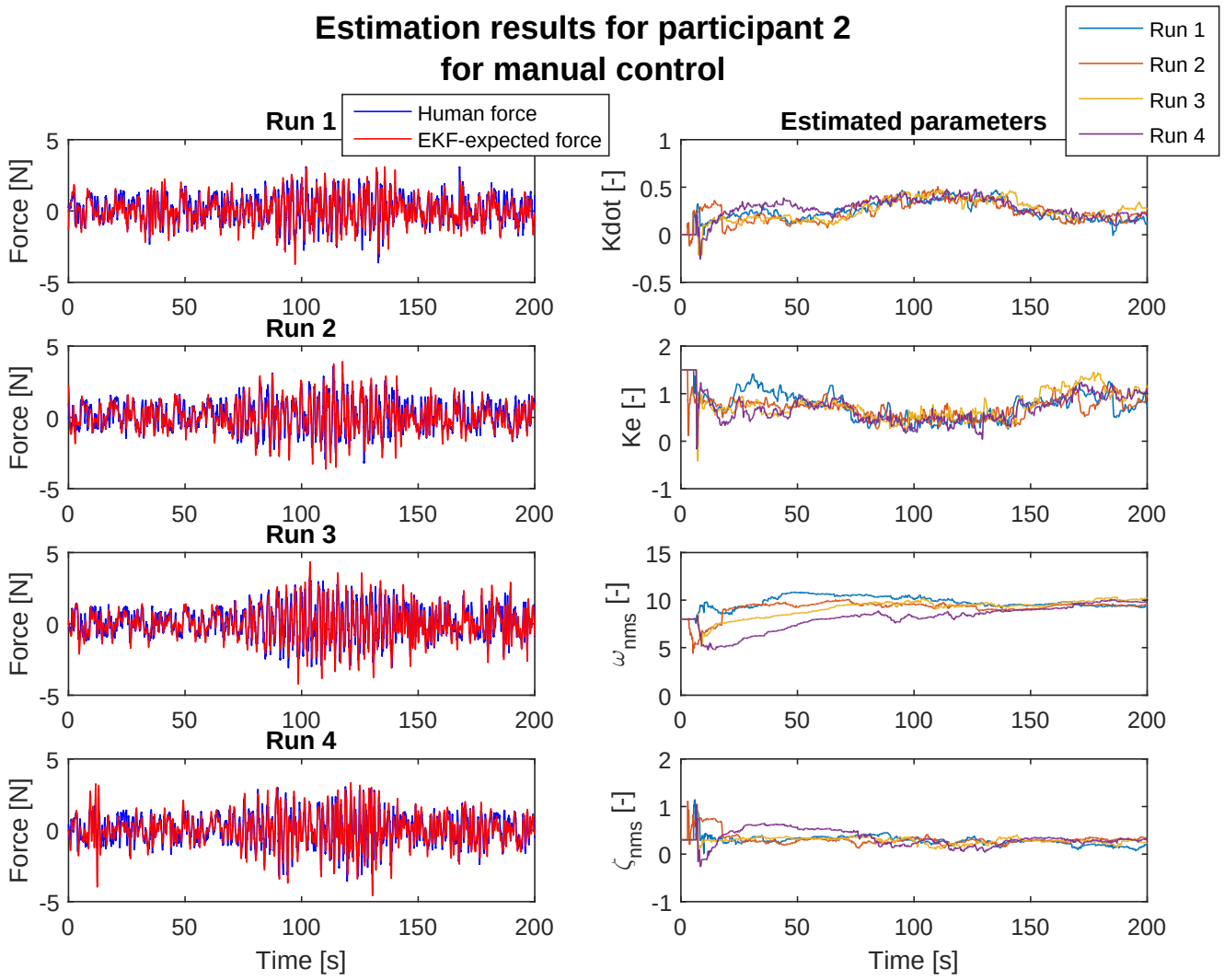

Fig. 34: Identification results participant 2, manual control

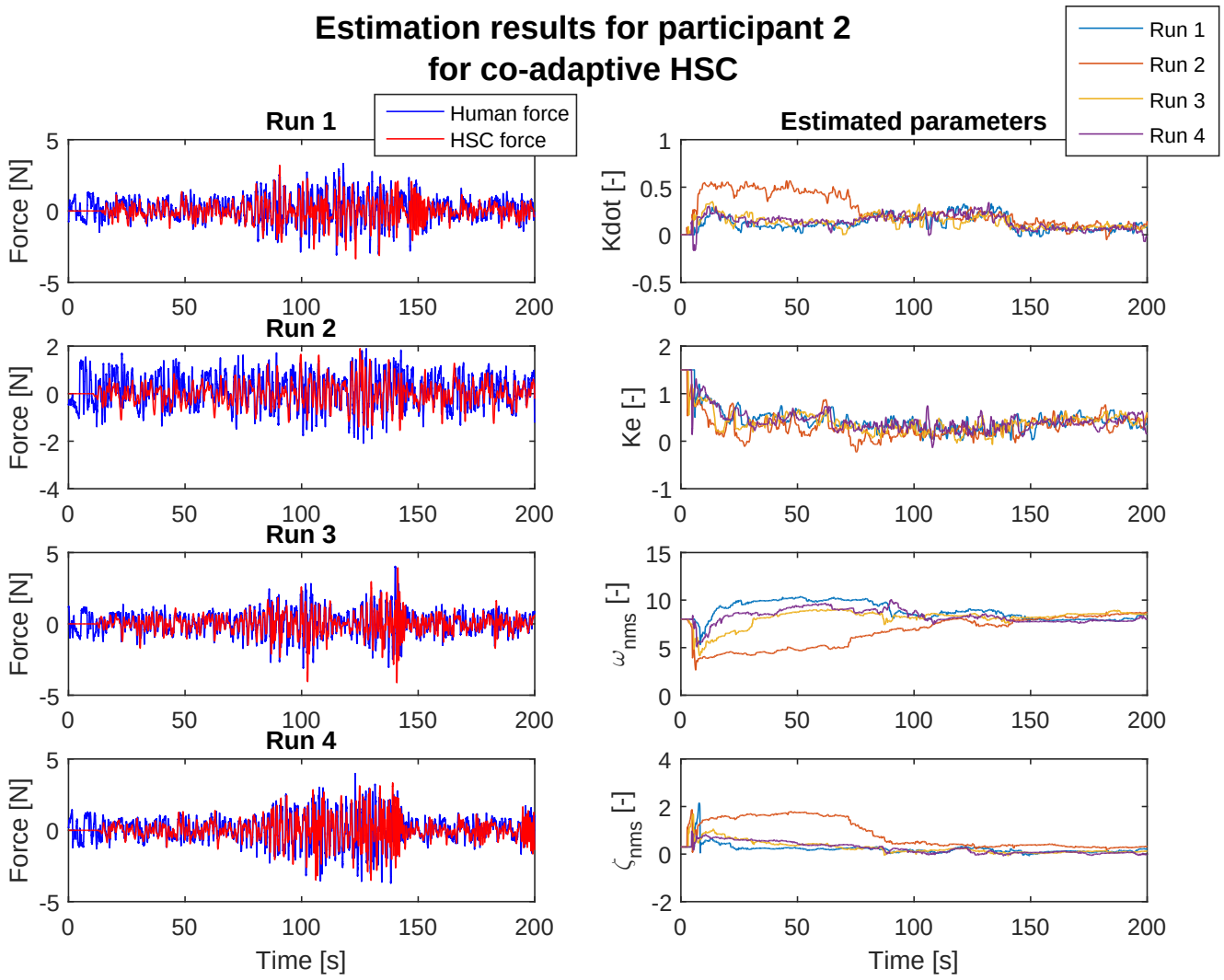

Fig. 35: Identification results participant 2, co-adaptive HSC

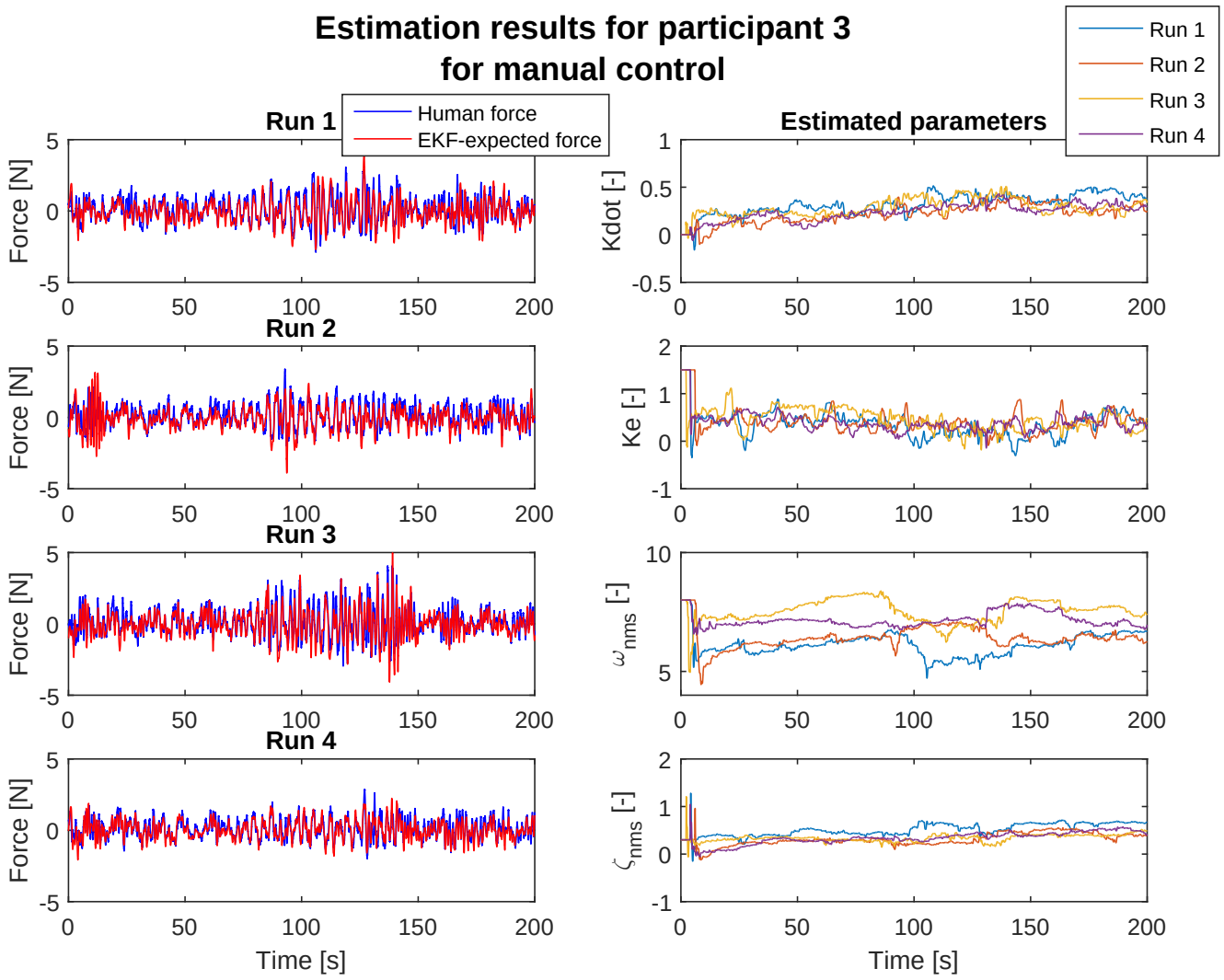

Fig. 36: Identification results participant 3, manual control

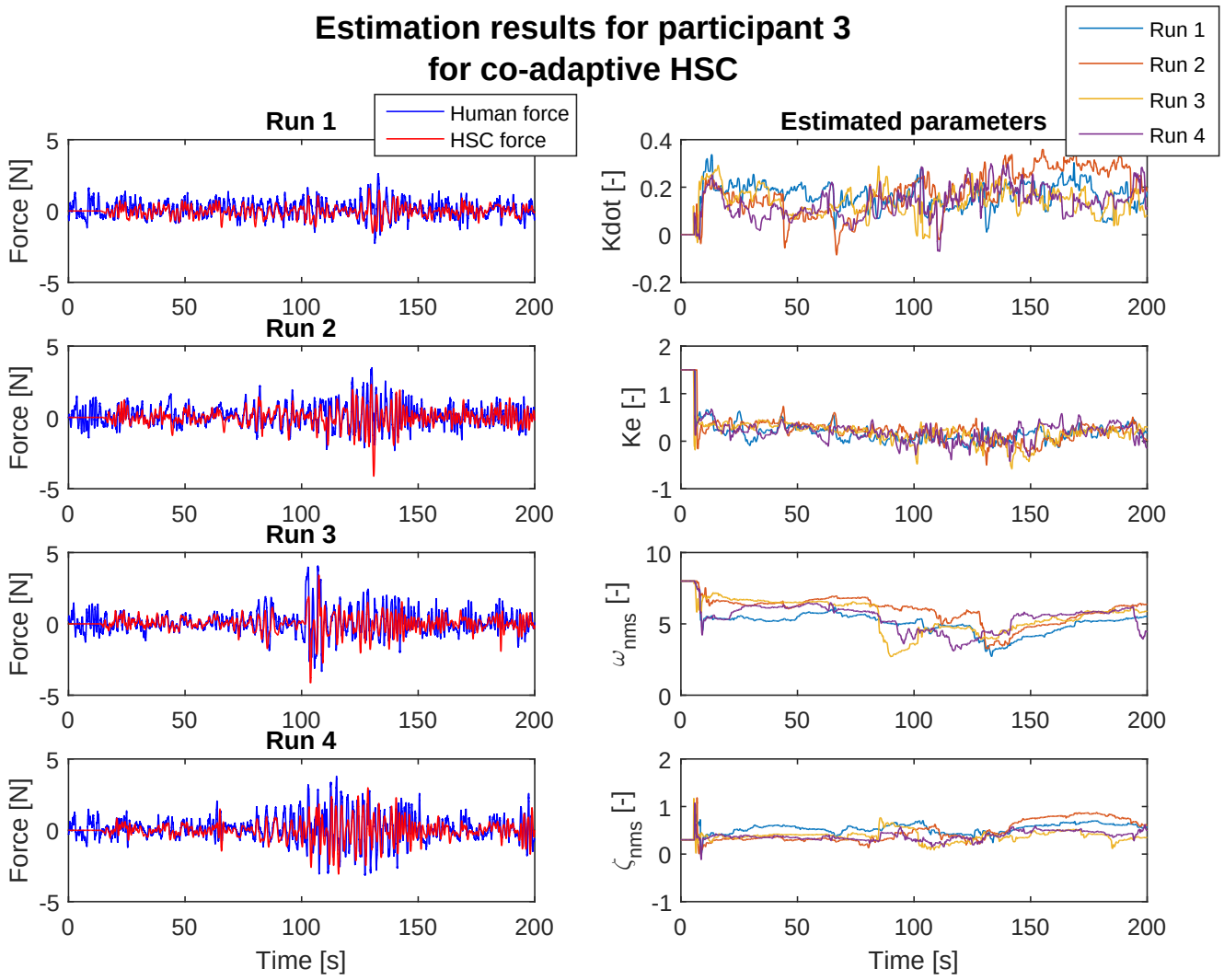

Fig. 37: Identification results participant 3, co-adaptive HSC

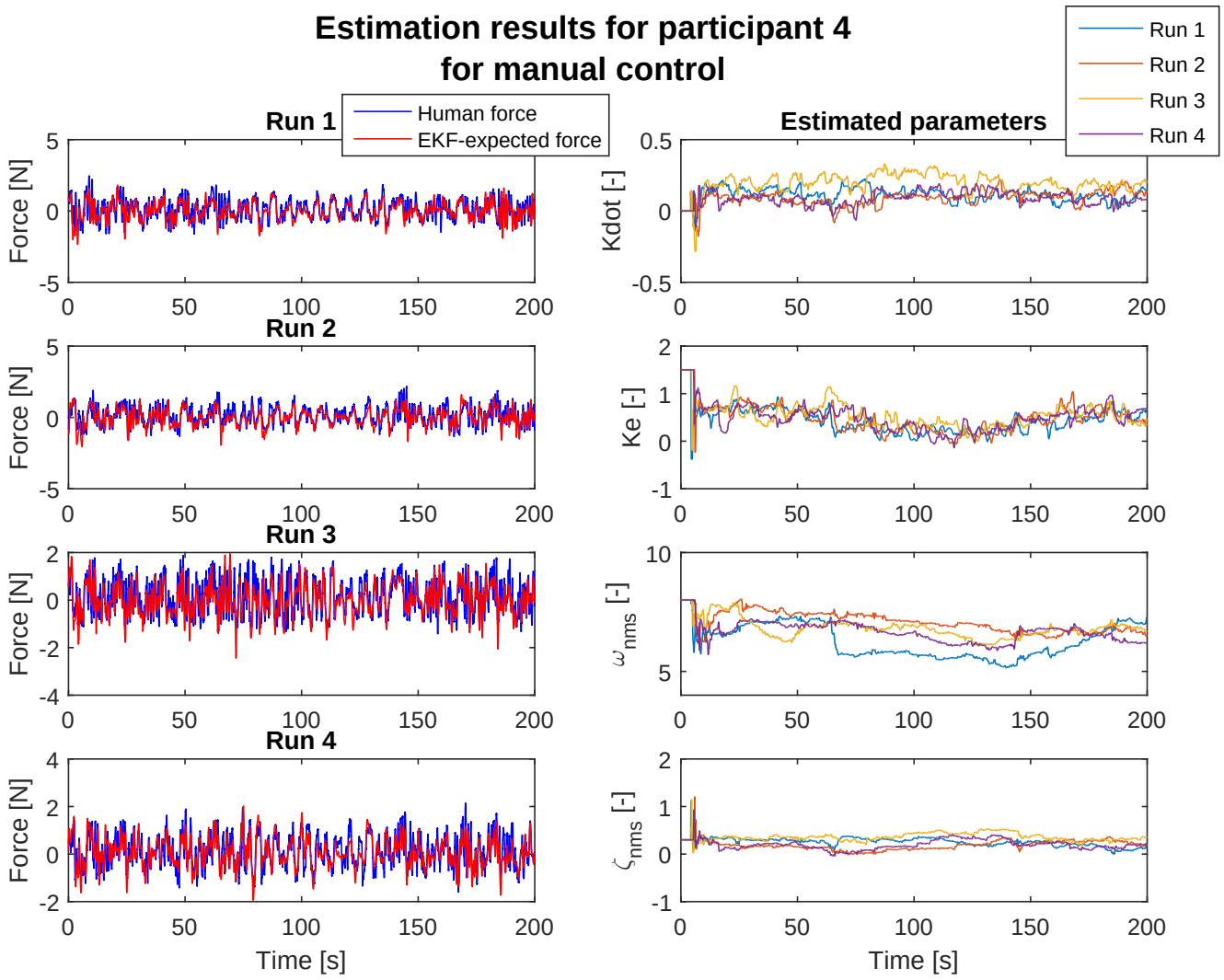

Fig. 38: Identification results participant 4, manual control

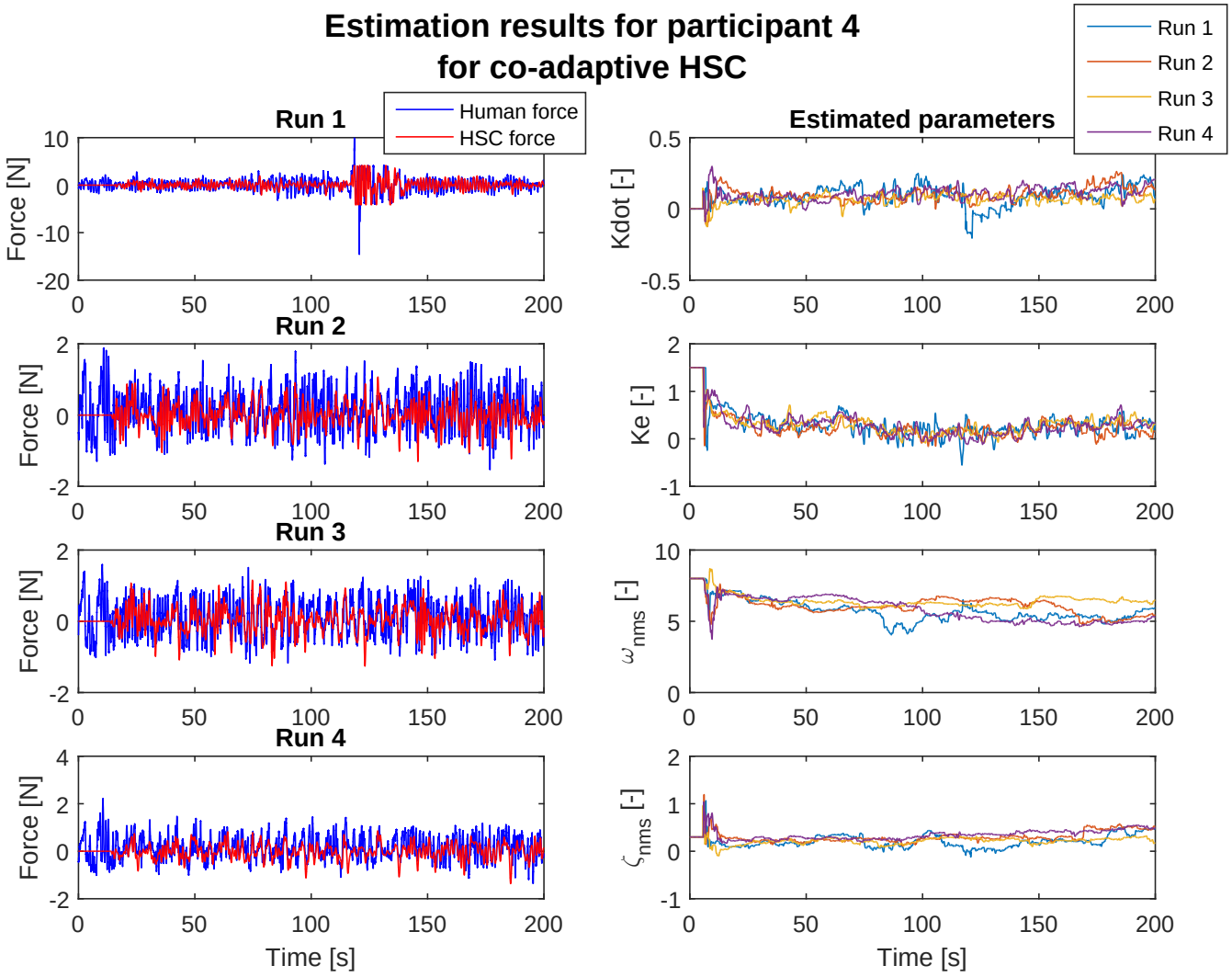

Fig. 39: Identification results participant 4, co-adaptive HSC

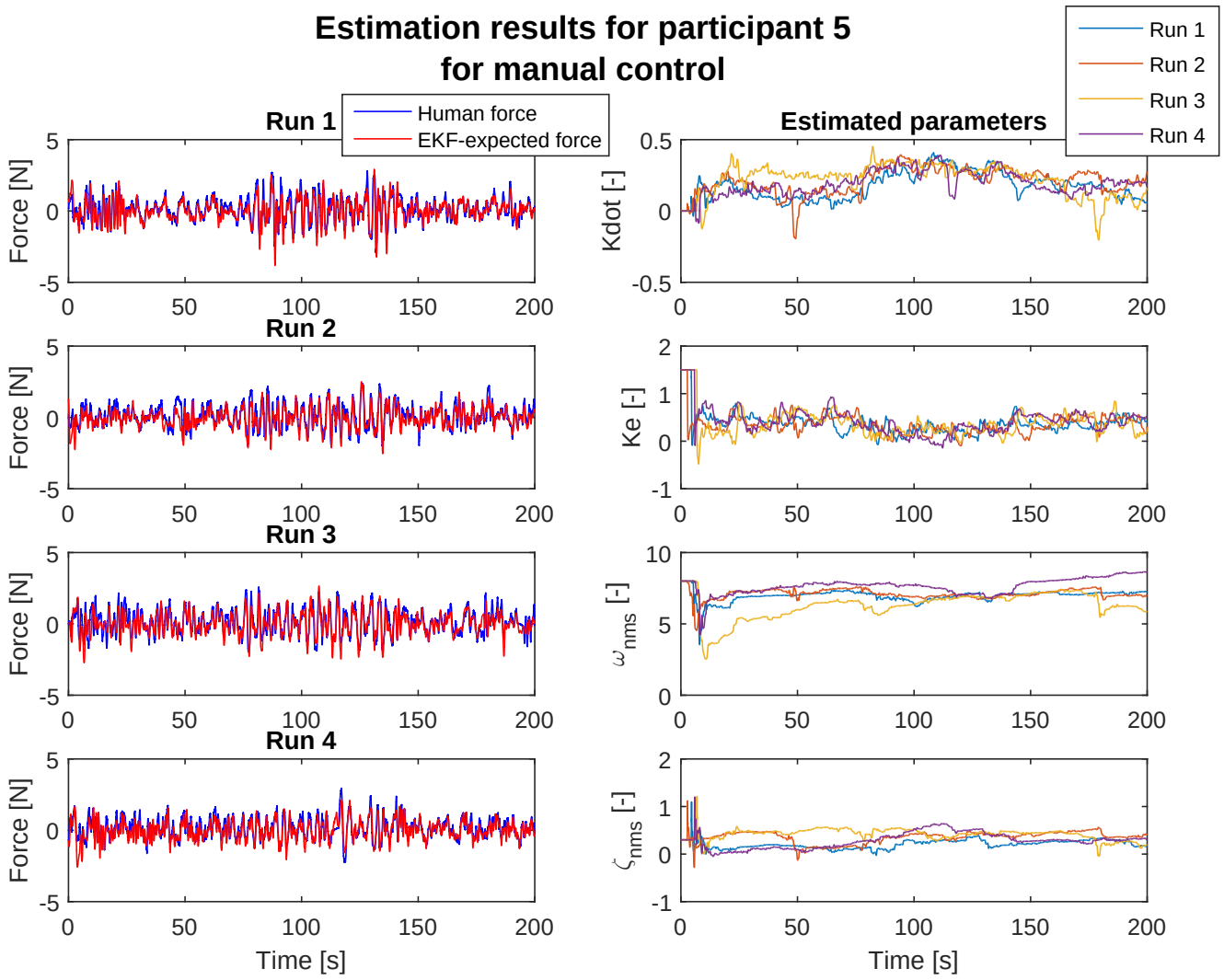

Fig. 40: Identification results participant 5, manual control

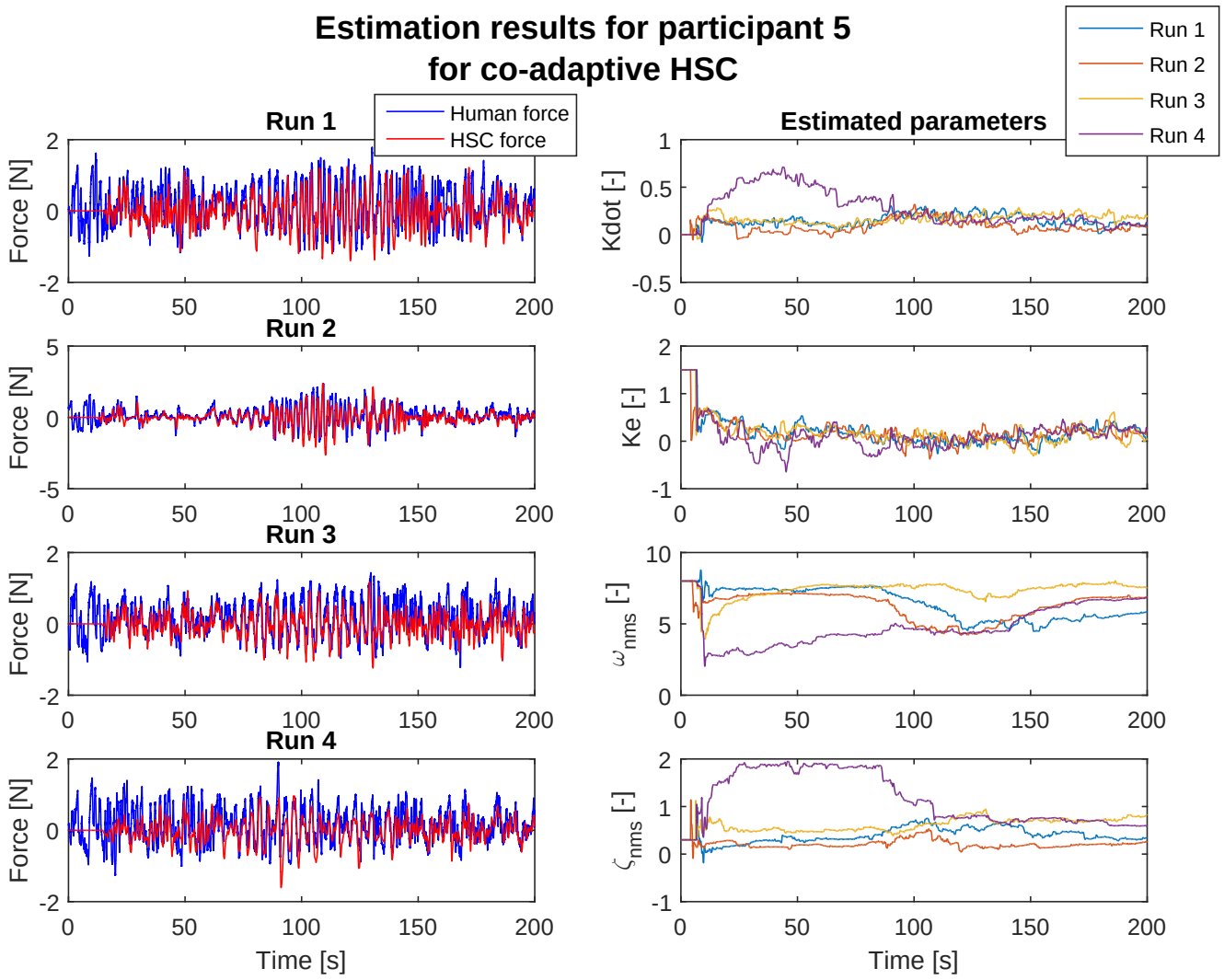

Fig. 41: Identification results participant 5, co-adaptive HSC

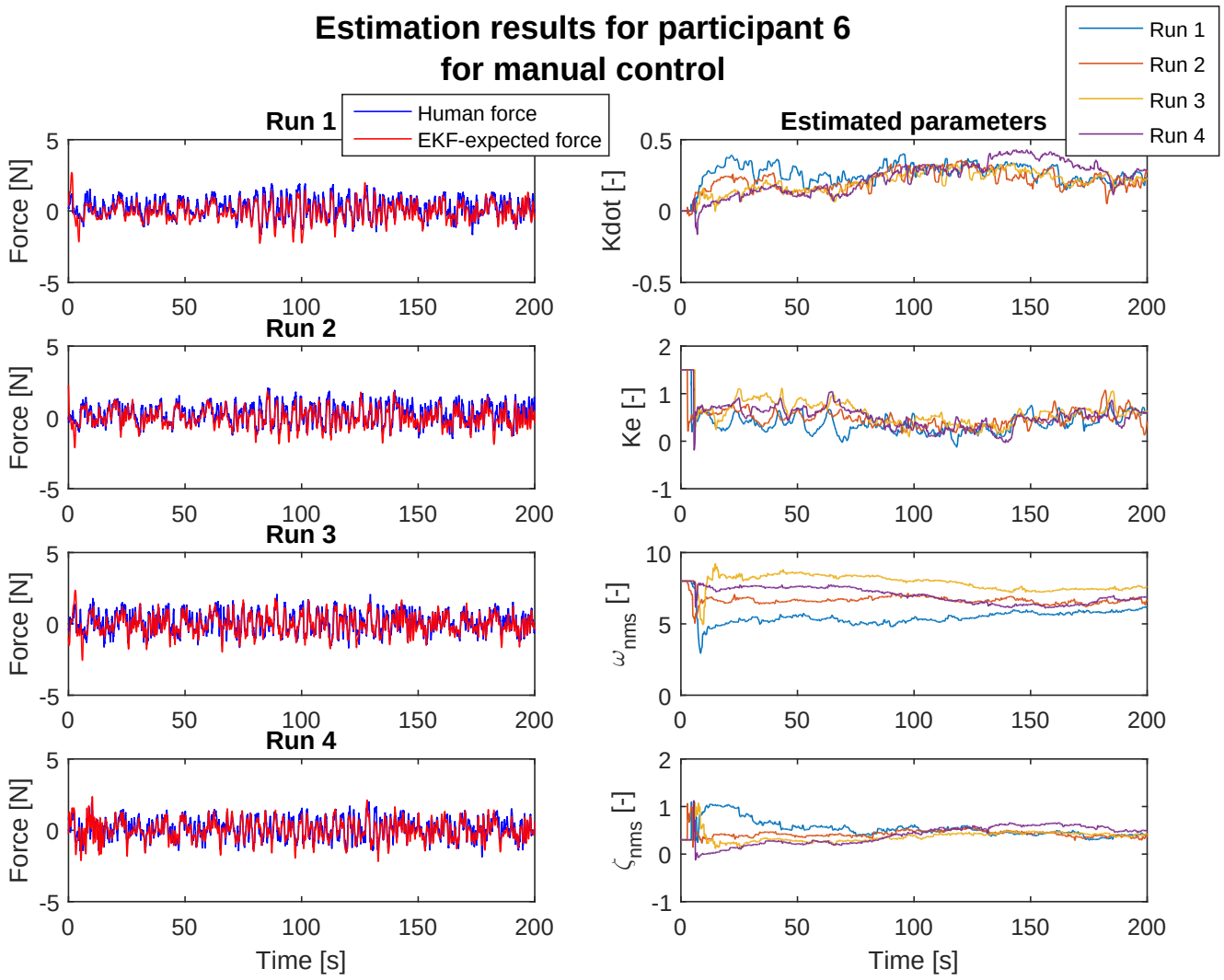

Fig. 42: Identification results participant 6, manual control

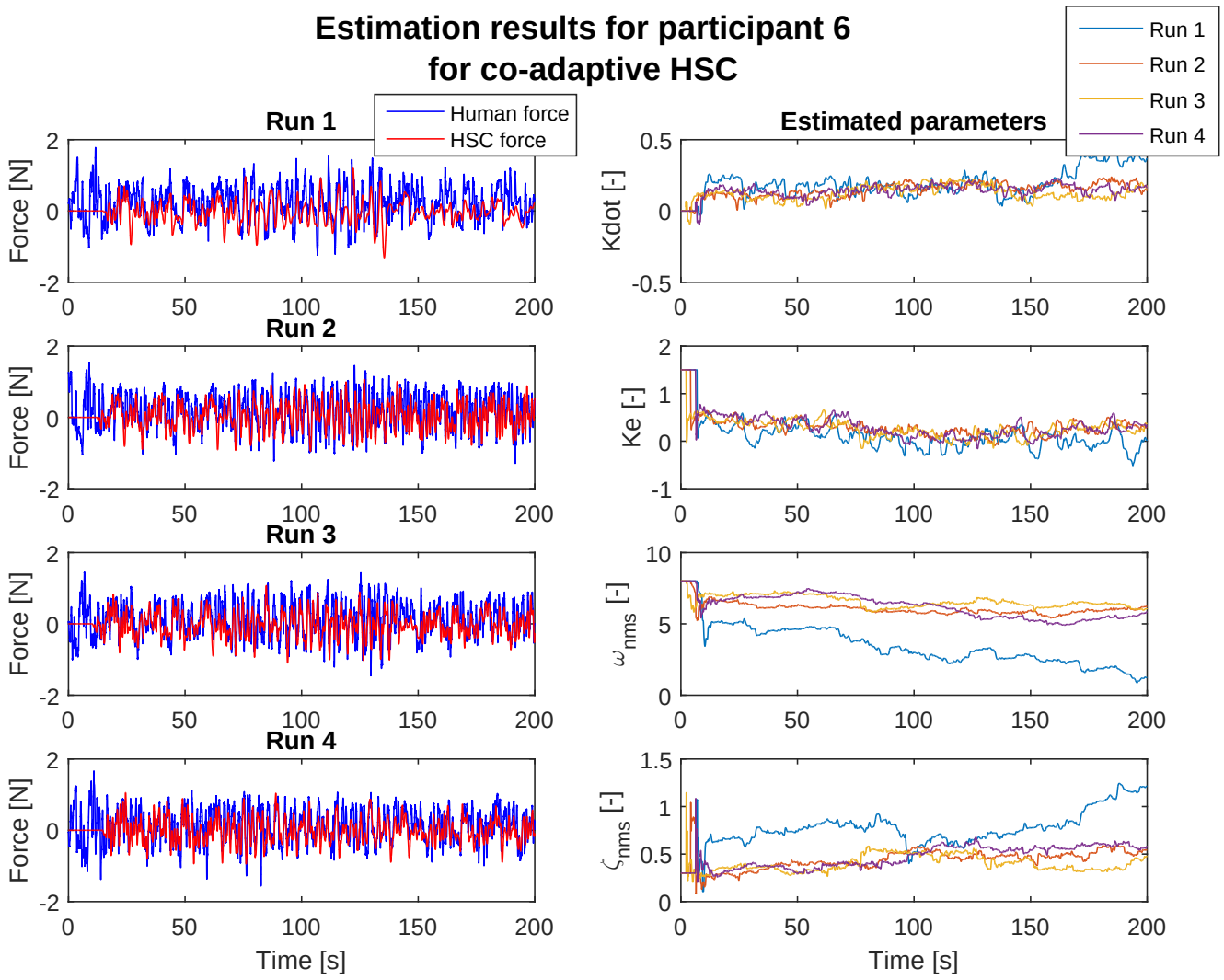

Fig. 43: Identification results participant 6, co-adaptive HSC

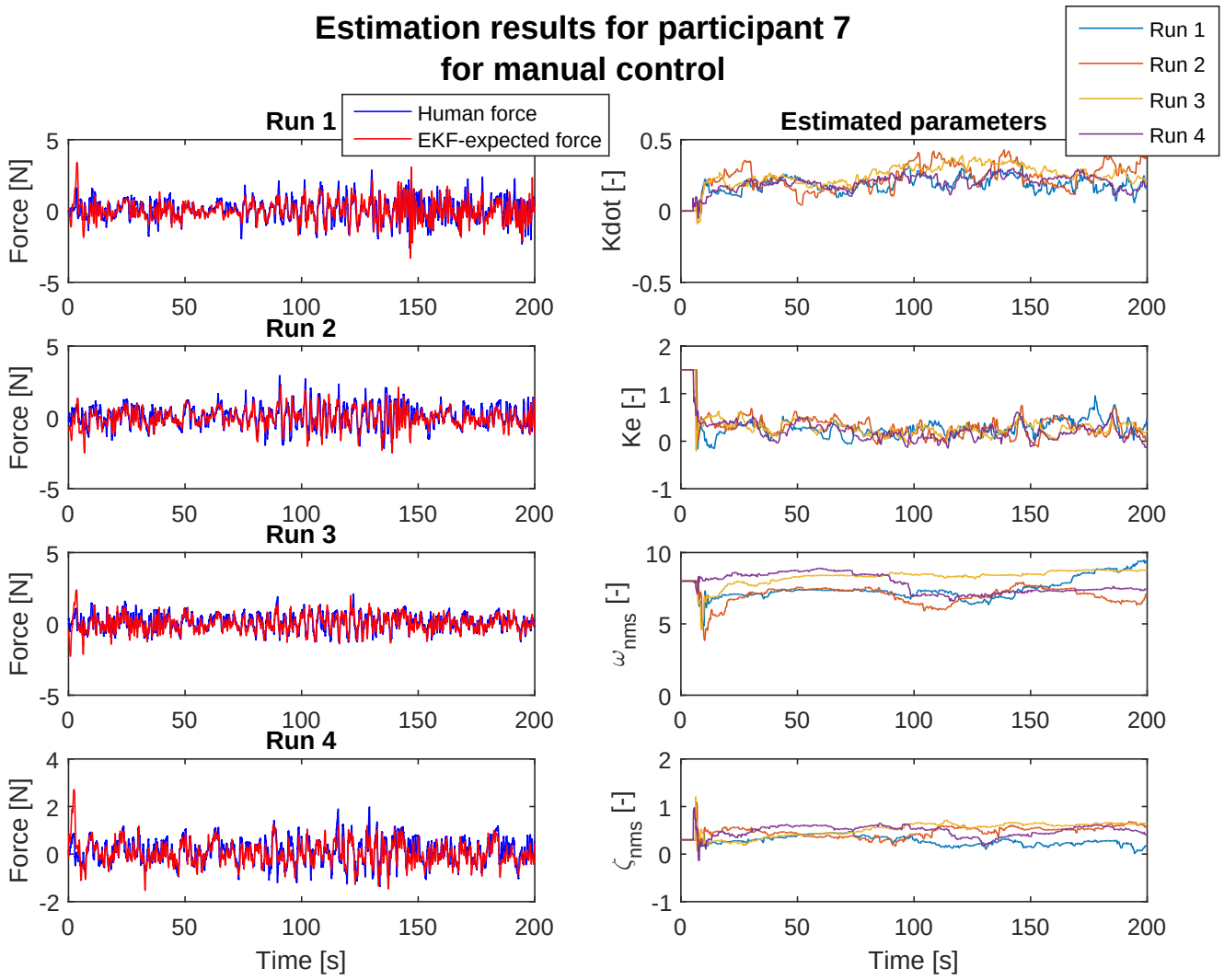

Fig. 44: Identification results participant 7, manual control

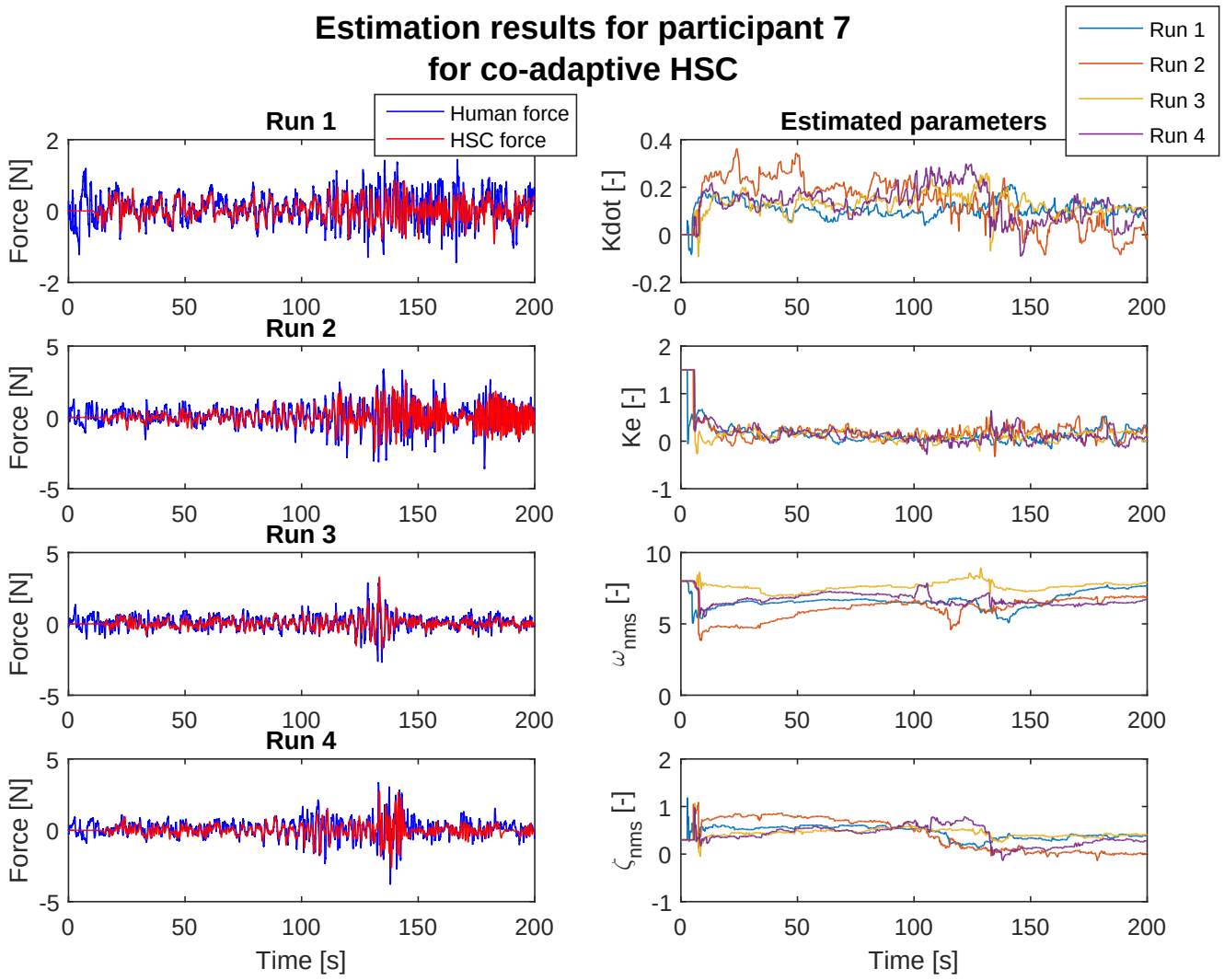

Fig. 45: Identification results participant 7, co-adaptive HSC

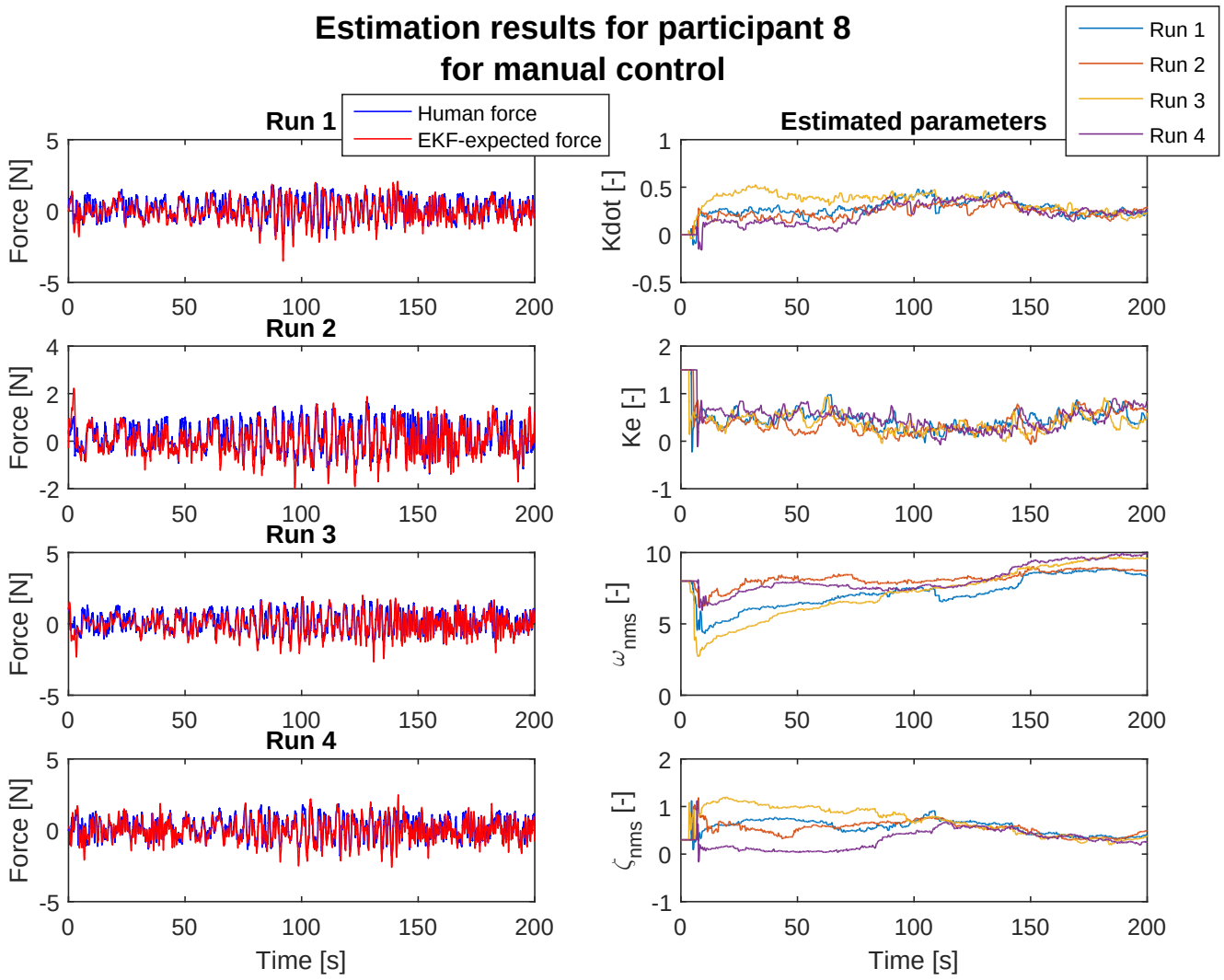

Fig. 46: Identification results participant 8, manual control

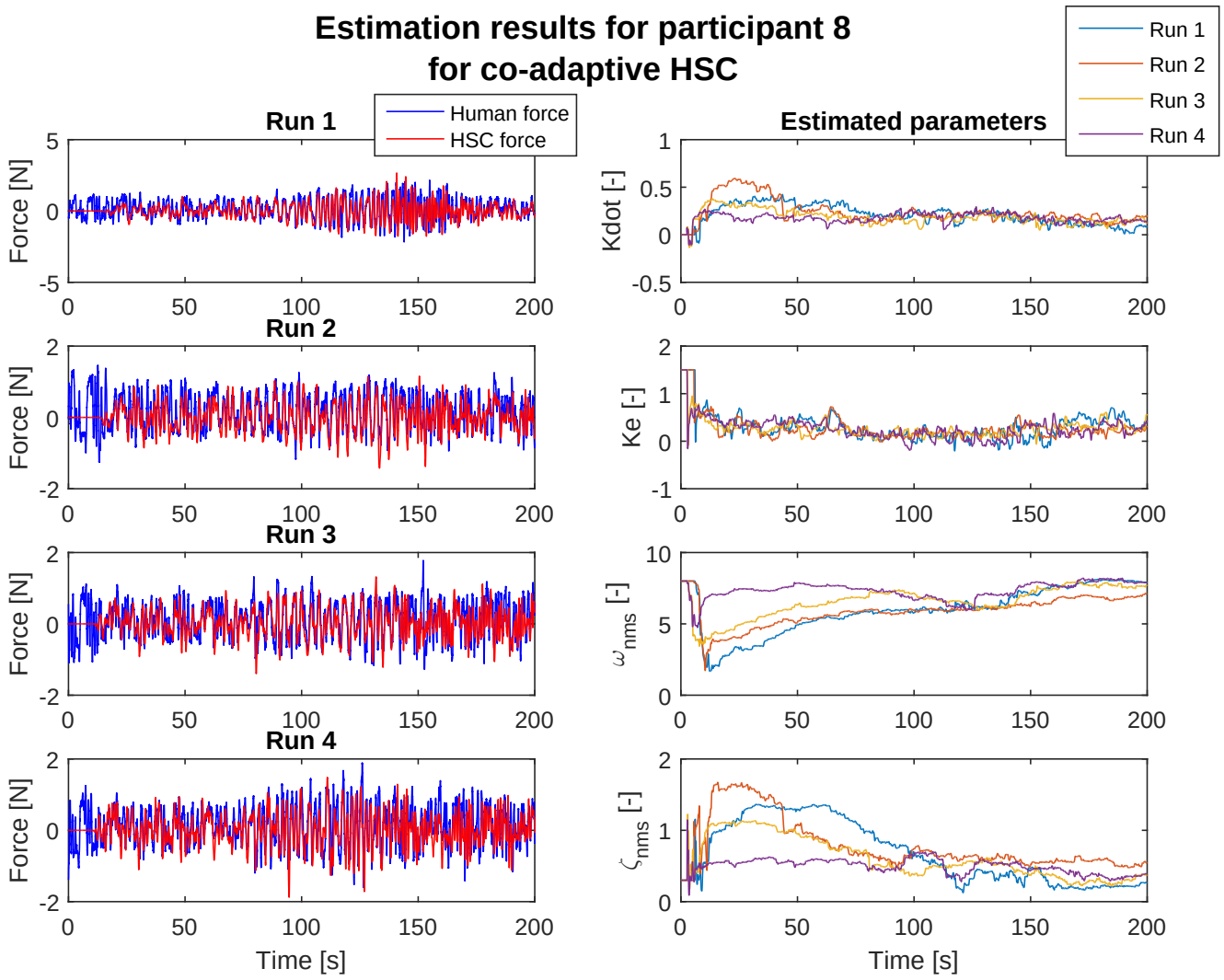

Fig. 47: Identification results participant 8, co-adaptive HSC

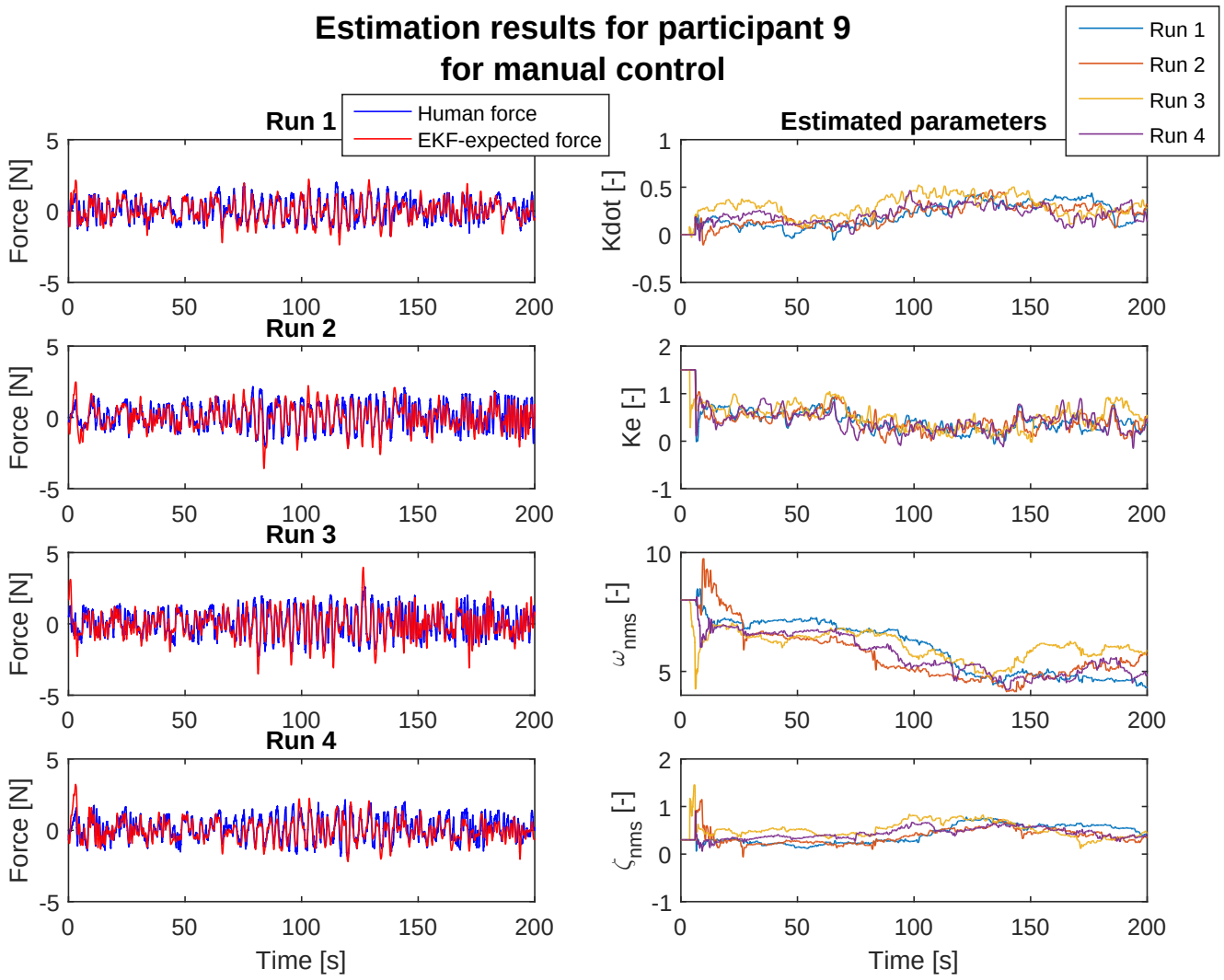

Fig. 48: Identification results participant 9, manual control

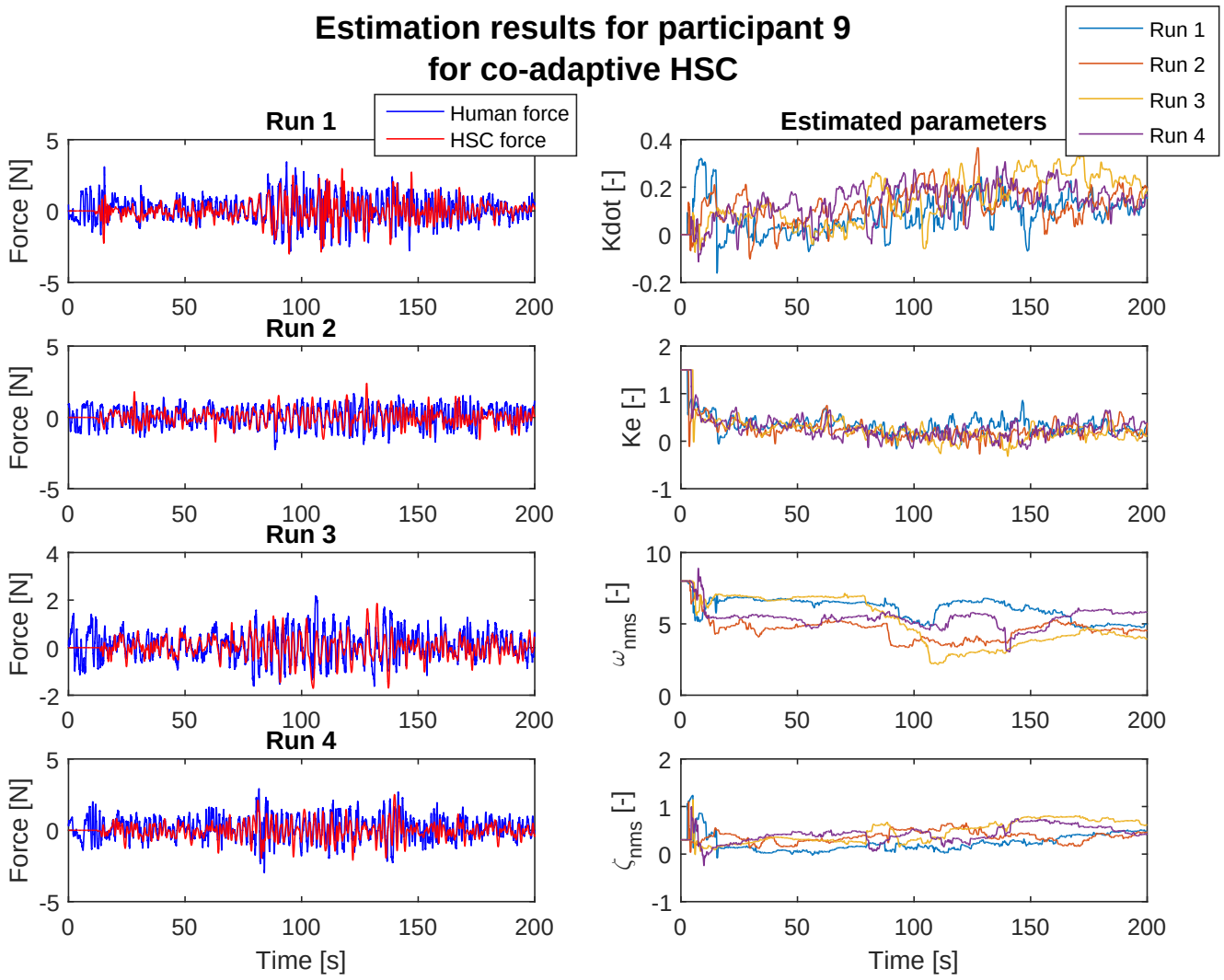

Fig. 49: Identification results participant 9, co-adaptive HSC

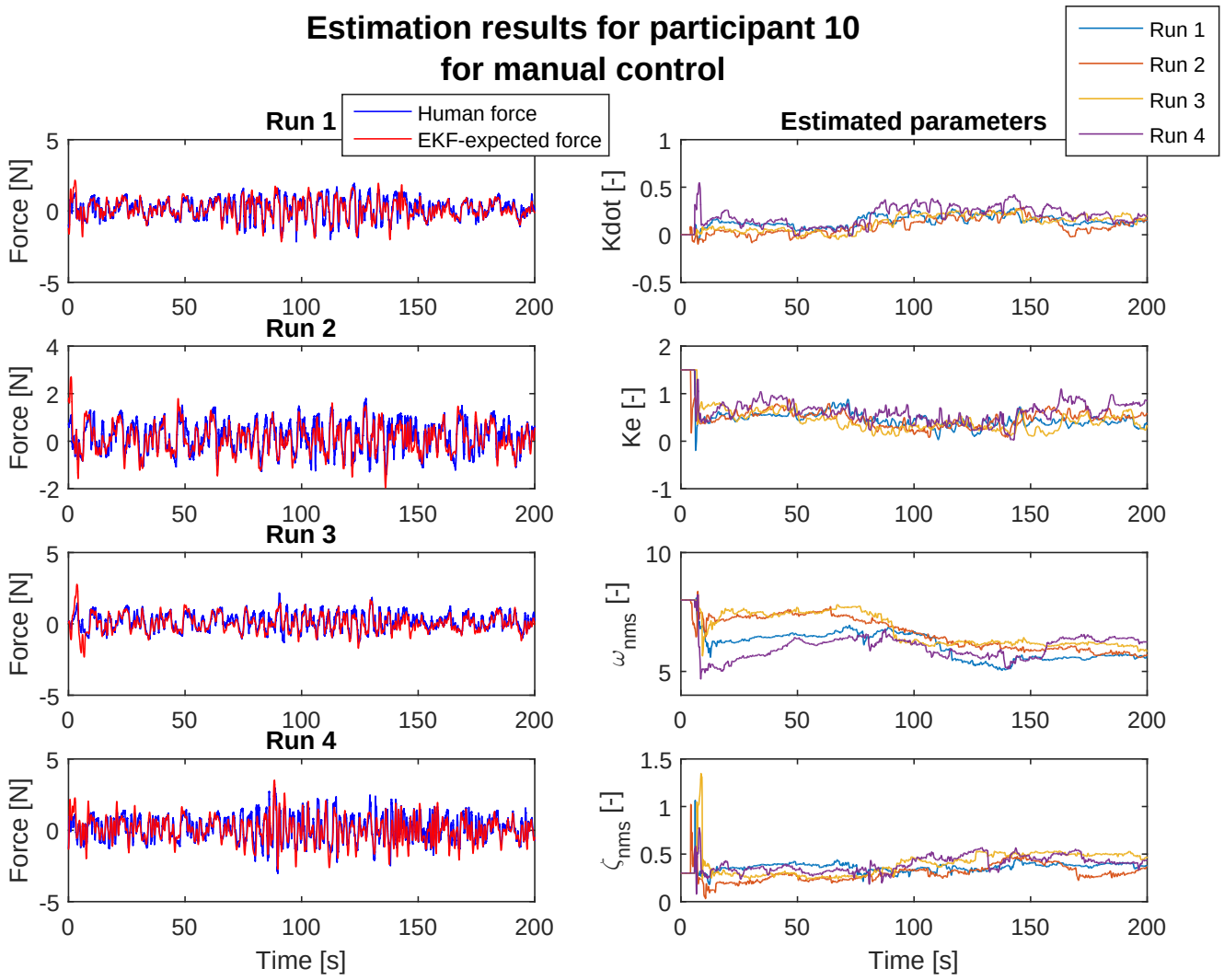

Fig. 50: Identification results participant 10, manual control

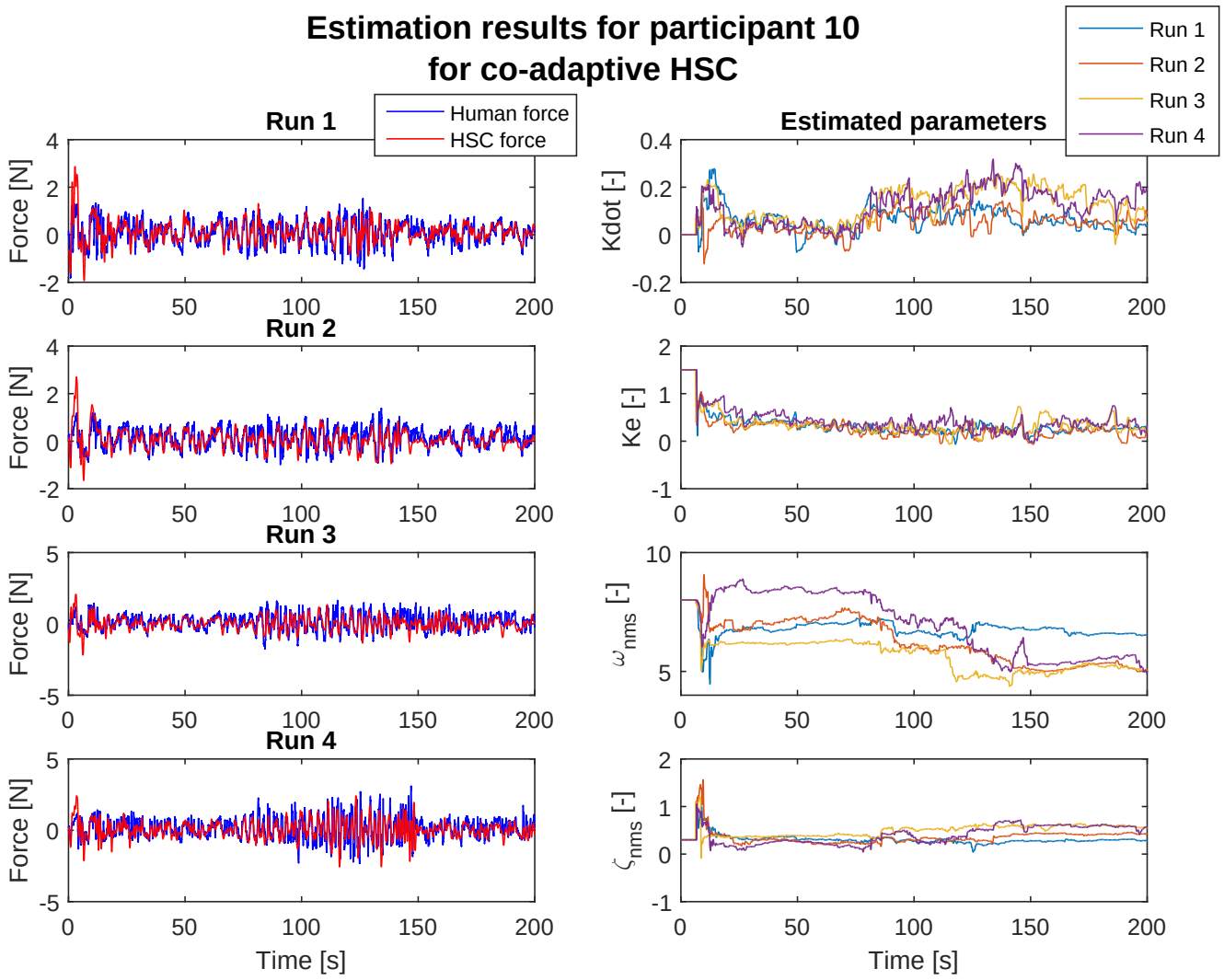

Fig. 51: Identification results participant 10, co-adaptive HSC

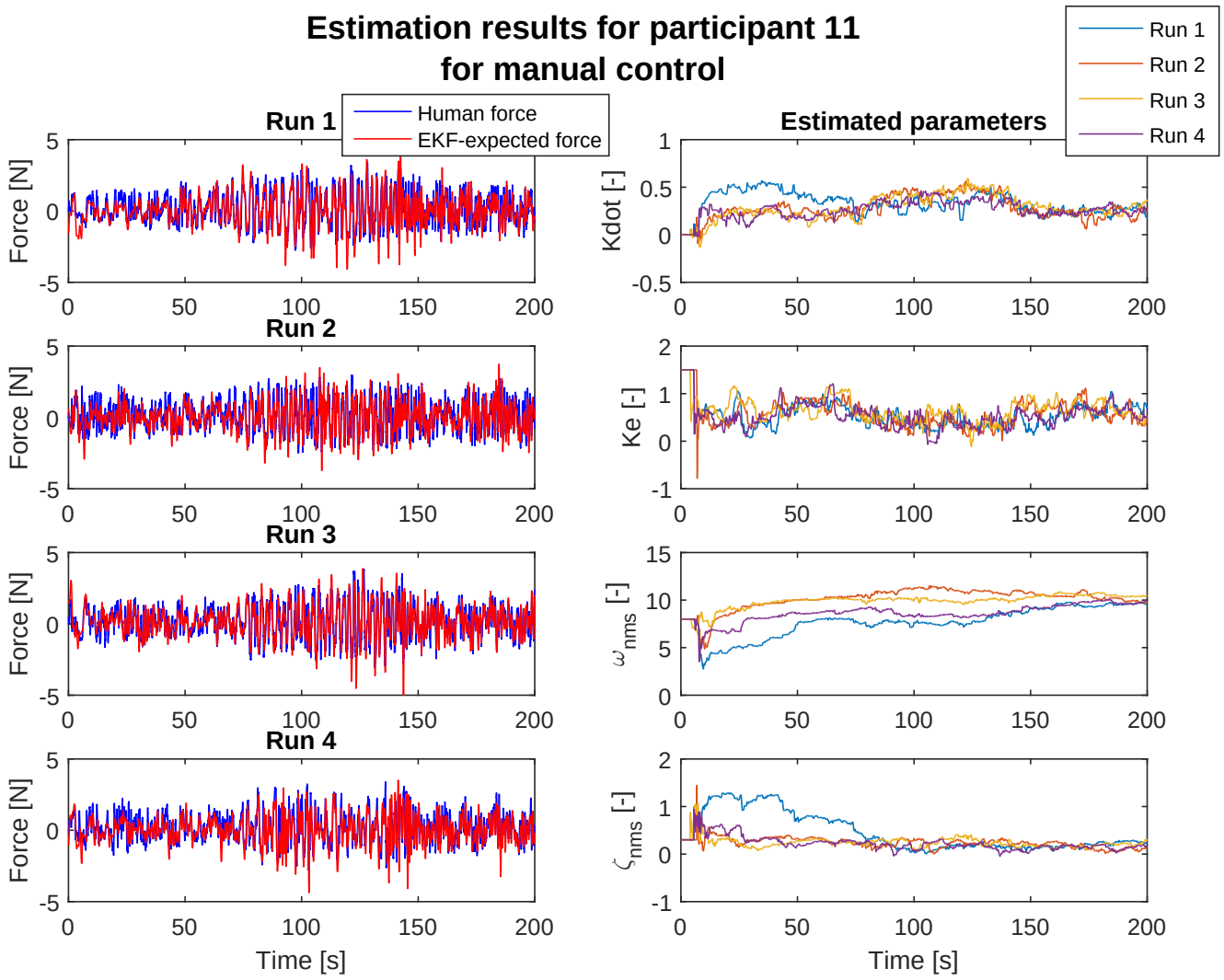

Fig. 52: Identification results participant 11, manual control

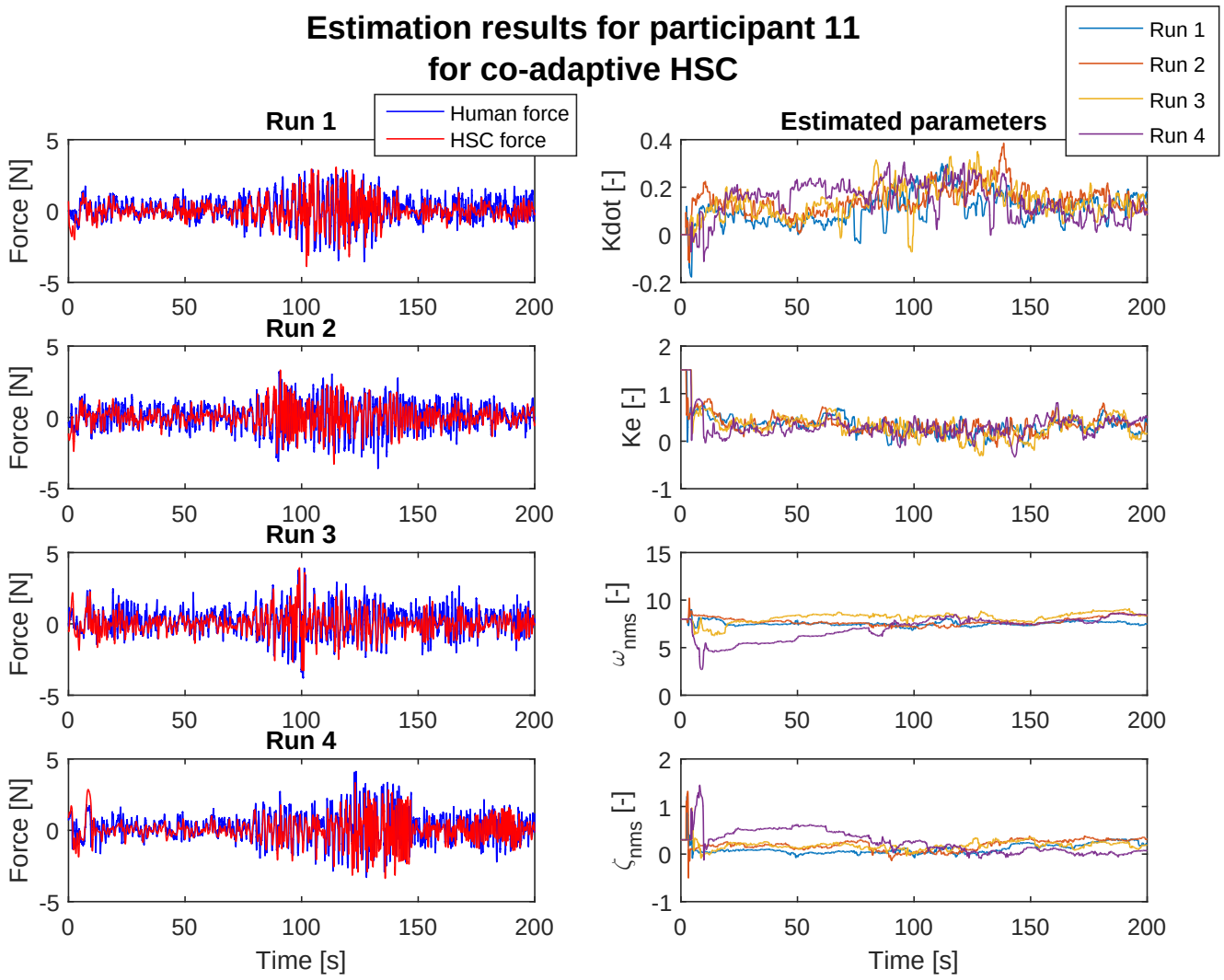

Fig. 53: Identification results participant 11, co-adaptive HSC